ACS EARTH AND SPACE CHEMISTRY

http://pubs.acs.org/journal/aesccq

Article

Global Distribution of the Phase State and Mixing Times within Secondary Organic Aerosol Particles in the Troposphere Based on Room-Temperature Viscosity Measurements

Adrian M. Maclean, Ying Li, Giuseppe V. Crescenzo, Natalie R. Smith, Vlassis A. Karydis, Alexandra P. Tsimpidi, Christopher L. Butenhoff, Celia L. Faiola, Jos Lelieveld, Sergey A. Nizkorodov, Manabu Shiraiwa, and Allan K. Bertram*

Cite This: *ACS Earth Space Chem.* 2021, 5, 3458−3473

Read Online

ACCESS | Metrics & More | Article Recommendations | Supporting Information

ABSTRACT: Information on the global distributions of secondary organic aerosol (SOA) phase state and mixing times within SOA is needed to predict the impact of SOA on air quality, climate, and atmospheric chemistry; nevertheless, such information is rare. In this study, we developed parameterizations for viscosity as a function of relative humidity (RH) and temperature based on room-temperature viscosity data for simulated pine tree SOA and toluene SOA. The viscosity parameterizations were then used together with tropospheric RH and temperature fields to predict the SOA phase state and mixing times of water and organic molecules within SOA in the troposphere for 200 nm particles. Based on our results, the glassy state can often occur, and the mixing times of water can often exceed 1 h within SOA at altitudes >6 km. Furthermore, the mixing times of organic molecules within SOA can often exceed 1 h throughout most of the free troposphere (i.e., $\gtrsim$1 km in altitude). In most of the planetary boundary layer (i.e., $\lesssim$1 km in altitude), the glassy state is not important, and the mixing times of water and organic molecules are less than 1 h. Our results are qualitatively consistent with the results from Shiraiwa et al. (Nat. Commun., 2017), although there are quantitative differences. Additional studies are needed to better understand the reasons for these differences.

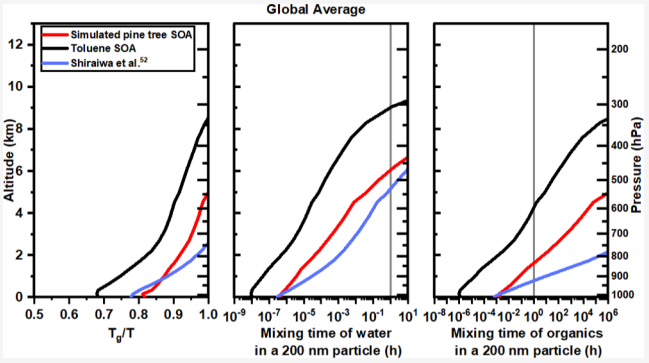

KEYWORDS: *viscosity, phase state, mixing time, secondary organic aerosol, toluene, Scots pine, free troposphere, planetary boundary layer*

1. INTRODUCTION

Secondary organic aerosol (SOA) is formed in the atmosphere via gas-phase and condensed-phase reactions.[1,2] SOA can impact Earth's climate both directly, by scattering incoming solar radiation, and indirectly, by serving as nuclei for liquid cloud droplets and ice particles.[3] SOA also contributes to poor air quality, which negatively impacts visibility and health.[4−6] It has been estimated that roughly 4.2 million deaths per year are the result of air pollution.[7,8]

Viscosity (η) is often used to specify the phase state of SOA, with $\eta < 10^2$ Pa s corresponding to a liquid, $\eta = 10^2$ to 10^{12} Pa s corresponding to a semisolid, and $\eta > 10^{12}$ Pa s corresponding to a glass.[9] If SOA is in a glassy state, it can act as nuclei for ice particles.[9−15] Furthermore, if the mixing time of water within a SOA particle is slow (greater than or equal to 1 h), then glassy SOA becomes more important as a nuclei for ice particles since the slow mixing of water within SOA means a glassy SOA core can persist longer in an air parcel updraft.[16] Hence, information on the global distribution of the phase state and mixing times of water within SOA is needed to determine when and where SOA particles can act as ice nuclei in the atmosphere.

Information on the global distribution of the mixing times of organics within SOA is also needed to predict aerosol growth, evaporation, and size distributions in chemical transport models.[17−23] If the mixing times of organics within SOA are less than or equal to roughly 1 h (the time step in global chemical transport models is often 0.5−1 h), equilibrium partitioning of semivolatile organic compounds to the particle phase is a reasonable assumption in these models. However, if the mixing times of organics are greater than roughly 1 h, nonequilibrium between semivolatile organic compounds and

Received: August 23, 2021
Revised: November 14, 2021
Accepted: November 16, 2021
Published: November 30, 2021

https://doi.org/10.1021/acsearthspacechem.1c00296
ACS Earth Space Chem. 2021, 5, 3458−3473

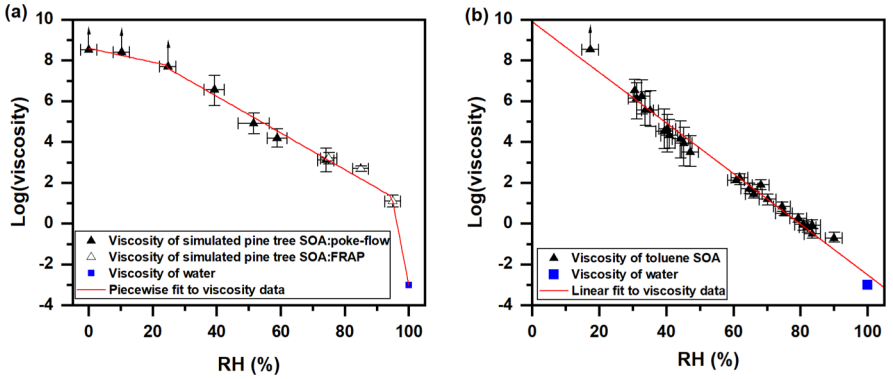

Figure 1. Panel a shows the log(viscosity) data from Smith et al.[58] as a function of the activity of water (RHs < 50%) and new measurements (RHs > 50%) using poke-flow and FRAP (Sections S1 and S2) for simulated pine tree SOA, the viscosity of pure water, as well as a fit to the data using eqs 1−3. Panel b shows the log(viscosity) data from Song et al.[48] as a function of the activity of water for toluene SOA, the viscosity of water, and a fit to the data using eq 6. For both panels, the *x*-error bars represent uncertainties in the RH measurements and the *y*-error bars correspond to the upper and lower limits of the viscosities. The points with upward arrows correspond to data where only lower limits of viscosity were obtained.

SOA should be considered. Slow mixing of organics within SOA can also influence the reactivity within SOA.[24−34]

The phase state and mixing times of water and organic molecules within SOA particles, or proxies of SOA particles, have been investigated in many laboratory studies.[35−49] These studies have shown that the glassy state can dominate, and mixing times of water and organics are slow in SOA and SOA proxies at low temperatures and low relative humidity (RH) values.[42,45−47] Mixing times of organic molecules within some types of SOA and SOA proxies can even exceed 1 h at room temperature if the RH is low (less than approximately 25%).[35,44,48] However, studies assessing the global distributions of SOA phase states and mixing times within SOA are rare.

Maclean et al.[50] investigated the global distribution of mixing times of organic molecules within SOA for the planetary boundary layer (PBL), the region of the atmosphere ranging from 0 to roughly 1 km in altitude, depending on the location and time.[51] To predict the mixing times, a parameterization of viscosity as a function of temperature and RH was developed based on room-temperature and low-temperature viscosity measurements. They found that the mixing times of organic molecules within SOA are commonly less than 1 h in the PBL. Shiraiwa et al.[52] investigated the global distribution of the phase state and mixing times of water and organic molecules within SOA for both the PBL and the free troposphere (FT) using a parameterization that related the glass transition temperature (T_g) to the molar mass and the oxygen-to-carbon ratio (O/C) of SOA components. They found that SOA is mostly in a glassy state, and the mixing times of water most often exceed 1 h in the middle and upper FT, while mixing of organic molecules often exceed 1 h throughout most of the FT. Regional air quality models were also applied to simulate SOA viscosity and T_g over the U.S., finding that a glassy state is ubiquitous in the FT.[53,54]

In the following, we investigate the global distribution of the phase state and mixing times of water and organic molecules within 200 nm SOA for both the PBL and FT. We focused on SOA with diameters of 200 nm since this is a common size of SOA particles in the troposphere.[55−57] Only one study, Shiraiwa et al.,[52] previously investigated global distributions in the FT. Our approach for calculating the phase state and mixing times is different from the approach taken by Shiraiwa et al.[52] In our case, we developed a parameterization for the viscosity of simulated pine tree SOA (proxy for biogenic SOA over the boreal forest) and toluene SOA (proxy for anthropogenic SOA) as a function of RH and temperature based on room-temperature viscosity measurements. This information, together with RH and temperature fields in the troposphere, was then used to estimate the global distribution of the phase state and mixing times in the PBL and FT for these types of SOA. Less parameters are required for our predictions compared to Shiraiwa et al.[52] For example, our method does not require information on the hygroscopicity or the Gordon−Taylor constants of the SOA, which have associated uncertainties leading to uncertainties in the predicted phase state and mixing times within SOA.[52] On the other hand, our method is associated with other limitations (see below), making our study complementary to the study by Shiraiwa et al.[52] We show that the glassy state and slow mixing times of water can be important at altitudes >6 km and that slow mixing of organic molecules can be important throughout most of the FT.

2. MATERIALS AND METHODS

To predict the global distributions of the SOA phase state and mixing times within SOA, we first developed parameterizations for the viscosity of simulated pine tree SOA (proxy for biogenic SOA over the boreal forest) and toluene SOA (proxy for anthropogenic SOA) as a function of RH and temperature based on laboratory viscosity measurements (Sections 2.1 and 2.2). Phase state and mixing times as a function of RH and temperature were then predicted from the RH- and temperature-dependent viscosities (Section 2.3). Finally, the global distributions of phase state and mixing times were determined using this information and average annual RH and temperature fields in the troposphere were extracted from the ECHAM/Modular Earth Submodel System Atmospheric Chemistry (EMAC) model (Section 2.5).

2.1. Parameterization for the Viscosity of Simulated Pine Tree SOA as a Function of RH and Temperature. We developed a parameterization for the viscosity of simulated pine tree SOA as a function of RH and temperature using the following data: (1) measured room-temperature viscosity data of SOA generated by the photooxidation of a mixture of volatile organic compounds (VOCs) representing emissions from healthy Scots pine (*Pinus sylvestris*) trees[58] and (2) room-temperature viscosity data of water.[59] These data are shown in

https://doi.org/10.1021/acsearthspacechem.1c00296
ACS Earth Space Chem. 2021, 5, 3458−3473

Figure 1a. The measured viscosities for the simulated Scots pine tree SOA at RH values less than or equal to 50% were taken from Smith et al.,[58] while the measured viscosities at RHs greater than 50% are based on new measurements discussed in the Supporting Information (Sections S1 and S2). The measured viscosities from Smith et al.[58] were based on the poke-flow technique, and the new measurements reported in the Supporting Information were based on the poke-flow technique and fluorescence recovery after photobleaching (FRAP). To determine viscosities from the poke-flow measurements, we used fluid simulations, which require material properties such as surface tension and slip length as the input.[44] However, these parameters are often not well constrained for the SOA material. As a result, conservative values were used in the simulations, which result in relatively large uncertainties in the viscosity data (Figure 1a).[58] The FRAP technique involved measuring diffusion coefficients of a large fluorescent dye within the SOA material and then converting these values to viscosity using the Stokes−Einstein equation. The Stokes−Einstein equation should be able to accurately predict viscosities from measured diffusion coefficients of large organic molecules in SOA since previous work has shown that the Stokes−Einstein equation can predict viscosities within the uncertainty of the measurements from diffusion coefficients when the radius of the diffusing molecule is similar to or greater than the radius of the matrix molecules.[39]

Healthy Scots pine trees emit VOCs dominated by monoterpenes with a small contribution from sesquiterpenes.[60] A mixture of α-phellandrene, β-pinene, α-pinene, 3-carene, camphene, and β-caryophyllene was used to simulate the tree emissions (see Table S1 in Smith et al.[58]). Pine trees are widely distributed throughout the boreal forest,[61] and Scots pine trees make up a significant portion of boreal forests in several European countries.[62] As a result, the simulated Scots pine tree SOA should be a good proxy for SOA over boreal forests, which represent the largest biome by area on earth. The applicability of these results to other types of biogenic SOA still needs to be determined. Simulated pine tree SOA was used as a proxy for biogenic SOA for this study in the place of more frequently used α-pinene SOA. Previous studies have found differences between SOA generated from multiple VOC precursors and the simpler model systems often used (α-pinene SOA).[63−66]

To generate a parameterization for viscosity as a function of RH and temperature, we first fit the data in Figure 1a piecewise to the following equations

$$\log(\eta(\mathrm{RH},\ 294\ \mathrm{K})) = \begin{cases} \left(1-\frac{\mathrm{RH}}{100}\right)a + \frac{\mathrm{RH}}{100}b, & \mathrm{RH} \le 24.75\ \% \quad (1) \\ \left(1-\frac{\mathrm{RH}}{100}\right)c + \frac{\mathrm{RH}}{100}d & 24.75 < \mathrm{RH} < 95\ \% \quad (2) \\ \left(1-\frac{\mathrm{RH}}{100}\right)e + \frac{\mathrm{RH}}{100}f, & \mathrm{RH} \ge 95\ \% \quad (3) \end{cases}$$

where η(RH, 294 K) is the RH-dependent viscosity at 294 K (i.e., room temperature) and a−f are fitting parameters. The values for coefficients [a, b, c, d, e, f] are [8.60 ± 0.16, 5.19 ± 0.90, 9.83 ± 0.33, 0.85 ± 0.21, 78.89, −3.02], respectively, based on the fitting. The results from the fitting are shown in Figure 1a (solid line). These equations were used since they monotonically decrease as the RH increases and since they fit the data well for their respective RH ranges. Equations 1−3 are equivalent to an activity-based viscosity mixing rule (see Supporting Information, Section S3) used previously with some success to predict viscosity in organic-water mixtures.[42]

To extrapolate the room-temperature viscosity data, η(RH, 294 K), to other temperatures, we used the Vogel−Tammann−Fulcher (VTF) equation

$$\eta(\mathrm{RH},\ T) = \eta_\infty e^{T_0(\mathrm{RH})D_f/T - T_0(\mathrm{RH})} \quad (4)$$

where η(RH, T) is the RH- and temperature-dependent viscosity, η_∞ is the viscosity at infinite temperature (10^{-5} Pa s based on Angell),[67,68] D_f is the fragility parameter, and T_0(RH) is the RH-dependent Vogel temperature. This is the same equation used by Shiraiwa et al.[52] to calculate viscosities as a function of temperature from the glass transition temperature. We first calculated T_0(RH) from the room-temperature viscosity parameterization discussed above by rearranging the VTF equation and evaluating at T = 294 K

$$T_0(\mathrm{RH}) = \frac{\ln\left(\frac{\eta(\mathrm{RH},\ 294\ \mathrm{K})}{\eta_\infty}\right)294\ \mathrm{K}}{D_f + \ln\left(\frac{\eta(\mathrm{RH},\ 294\ \mathrm{K})}{\eta_\infty}\right)} \quad (5)$$

To be consistent with Shiraiwa et al.,[52] we assumed D_f = 10. The fragility parameter for organic compounds is typically in the range of ∼5−30.[69] Furthermore, for molar masses greater than 200 g mol^{-1}, D_f is typically in the range of 5−20 and approaches a limit of ∼10 at molar masses greater than 400 g mol^{-1}.[70] The value of D_f was assumed to be independent of RH.[52,70−72] This assumption was consistent with previous studies which found that the values of D_f in sucrose and citric acid were independent of water content, except when the water content was very low.[68,73,74] After T_0(RH) was calculated, we calculated η(RH, T) using eq 4.

2.2. Parameterization for the Viscosity of Toluene SOA as a Function of RH and Temperature. We developed a parameterization for the viscosity of toluene SOA (proxy of anthropogenic SOA) as a function of RH and temperature using the following data: (1) measured room-temperature viscosity data of SOA generated via the photo-oxidation of toluene[48] and (2) room-temperature viscosity data of water.[59] These data are shown in Figure 1b. Aromatic hydrocarbons (including toluene) are an important source of SOA in urban environments,[75,76] and toluene SOA is often used as a proxy for anthropogenic SOA.[77,78] Furthermore, the RH-dependent viscosity of toluene SOA is similar to the RH-dependent viscosity of SOA generated from diesel fuel vapors.[79] Diesel fuel vapors contain a mixture of VOCs, and SOA generated from these vapors is likely a good proxy for SOA from anthropogenic sources.[75,80−83]

To generate a parameterization for the viscosity of toluene SOA as a function of RH and temperature, we first fit the data in Figure 1b to an activity-based viscosity mixing rule (eq 6)

$$\log(\eta(\mathrm{RH},\ 294\ \mathrm{K})) = \left(1-\frac{\mathrm{RH}}{100}\right)g + \frac{\mathrm{RH}}{100}h \quad (6)$$

The value of coefficients [g, h] are [9.89 ± 0.20, −2.52 ± 0.15], respectively, based on the fitting. The results of the fitting are included in Figure 1b (solid line). Equation 6 was used to fit the data since the logarithm of viscosity

https://doi.org/10.1021/acsearthspacechem.1c00296
ACS Earth Space Chem. 2021, 5, 3458−3473

monotonically decreases as the RH increases and it fit the data well. To extrapolate the room-temperature viscosity data, η(RH, 294 K), to other temperatures, we used the same approach discussed above for simulated pine tree SOA.

2.3. Predicting Phase State and Mixing Times. To determine if the SOA was in a glassy state, we first calculated the glass transition temperature of the SOA as a function of RH using the following equation

$$T_g(\mathrm{RH}) = \frac{T_0(\mathrm{RH}) \times (D_f + 39.17)}{39.17} \quad (7)$$

where T_g(RH) is the RH-dependent glass transition temperature of the SOA. Equation 7 was derived using the VTF equation (eq 4) and assuming $\eta = 10^{12}$ Pa s at the glass transition temperature.[67,68,70] Next, the variable $T_g(\mathrm{RH})/T$ was evaluated, and a $T_g(\mathrm{RH})/T$ value ≥1 was assumed to correspond to the glassy state.

To determine the mixing times of organic molecules within SOA, we first calculated the diffusion coefficients of organic molecules within SOA as a function of temperature and RH from η(RH, T) using the Stokes−Einstein equation

$$D_{org}(\mathrm{RH}, T) = \frac{kT}{6\pi\eta_{org}(\mathrm{RH}, T)R_{diff}} \quad (8)$$

where D_{org}(RH, T) is the RH- and temperature-dependent diffusion coefficient of organic molecules within SOA, η_{org} is the RH- and temperature-dependent viscosity of the SOA, k is the Boltzmann constant, and R_{diff} is the radius of the diffusing molecules. Although the Stokes−Einstein equation drastically underpredicts the diffusion coefficients of water and small oxidants in organic−water mixtures, it predicts diffusion coefficients within the uncertainty of the measurements for the majority of the cases reported in the literature when the radius of the diffusing molecule (R_{diff}) is greater than or equal to the radius of the matrix molecules (R_{matrix}).[39] The value of R_{matrix} represents the average radius of the organic molecules that make up the SOA particles, whereas R_{diff} represents the radius of the molecules of interest diffusing through the SOA. For the case of organic diffusion, we assumed $R_{diff} = R_{matrix}$, meaning that the radius of the diffusing molecules was the same as the average radius of the SOA molecules. For our calculations, we used a R_{diff} value of 0.4 nm, which was consistent with molecular weights, densities, and an assumed spherical geometry of SOA molecules.[44,58,84−91] In contrast, Shiraiwa et al.[52] used a value of 0.1 nm for the radius of the diffusing organic molecules. This results in a difference of only a factor of 4 in the mixing times of organic molecules according to eq 8, which is small compared to the variability in the mixing times considered here (greater than 5 orders of magnitude in variability). Nevertheless, when comparing our results with Shiraiwa et al.,[52] all of the organic mixing times from Shiraiwa et al.[52] were increased by a factor of 4 to be consistent with the radius of the diffusing molecules used in our study.

After determining D_{org}(RH, T), we calculated the mixing times of organic molecules as a function of RH and temperature, $\tau_{mix,org}$(RH, T), using the following equation[92]

$$\tau_{mix,org}(\mathrm{RH}, T) = \frac{d_p^2}{4\pi^2 D_{org}(\mathrm{RH}, T)} \quad (9)$$

where d_p is the diameter of the SOA particle. The diameter of the SOA particle was assumed to be 200 nm as that is a common size of SOA particles in the atmosphere.[55−57] This mixing time corresponds to the time it takes for the concentration of the diffusing species at the center of the particle to reach ∼37% ($1/e$) of the equilibrium concentration.

To determine the mixing times of water within SOA, the diffusion coefficients of water as a function of RH and temperature were determined using the fractional Stokes−Einstein equation[38,39,93]

$$D_{H_2O}(\mathrm{RH}, T) = D_0(T) \times \left(\frac{\eta_0(T)}{\eta(\mathrm{RH}, T)}\right)^{\xi} \quad (10)$$

where D_{H_2O}(RH, T) is the RH- and temperature-dependent diffusion coefficient of water in SOA, $D_0(T)$ is the temperature-dependent diffusion coefficient of water in pure water, ξ is the fractional exponent, and $\eta_0(T)$ is the temperature-dependent viscosity of pure water. The temperature-dependent viscosity data for pure water were taken from Hallett[94] and Crittenden et al.[59] Details can be found in Section S4. $D_0(T)$ was evaluated using the Stokes−Einstein equation and assuming the radius of a molecule of water to be 0.1 nm.[93] The value of the fractional exponent was calculated using eq 11[38]

$$\xi = 1 - \left[A \exp\left(-B\frac{R_{diff}}{R_{matrix}}\right)\right] \quad (11)$$

where A and B are coefficients with values of 0.73 and 1.79, respectively. To evaluate eq 11, we assumed R_{diff} = 0.1 nm and R_{matrix} = 0.4 nm to be consistent with the size of water and organic molecules, respectively, as discussed above. The fractional Stokes−Einstein equation (eq 10) combined with eq 11 was able to predict 98% of the published diffusion coefficients of small molecules, including water, within the uncertainties of the measurements for organic−water mixtures.[38] Once D_{H_2O}(RH, T) was determined using eqs 10 and 11, we then calculated the mixing times of water within the SOA using an equation similar to eq 9. To calculate the diffusion coefficients of water, we used the fractional Stokes−Einstein equation in place of the method used by Shiraiwa et al.[52] because the fractional Stokes−Einstein equation does not require any assumption about the hygroscopicity or density of the SOA, unlike the method used by Shiraiwa et al.[52]

2.4. Predicting the Phase State and Mixing Times from Shiraiwa et al.[52] Shiraiwa et al.[52] used the EMAC atmospheric chemistry-climate model which includes the organic aerosol module ORACLE to simulate the mass of biogenic and anthropogenic SOA in four separate volatility bins.[95,96] Each volatility bin was then assigned molar masses and oxygen-to-carbon ratios (O/C) based on the molecular corridor approach.[97] The glass transition temperature (T_g) for each bin was then calculated from the molar mass and O/C using a parameterization developed by Shiraiwa et al.[52] The glass transition temperature as a function of RH of the total SOA (biogenic and anthropogenic SOA combined) was then calculated from the glass transition temperature of each volatility bin and the Gordon−Taylor approach. Viscosities and mixing times were then calculated as a function of temperature and RH from the RH-dependent glass transition temperature of the total SOA. One consequence of this

https://doi.org/10.1021/acsearthspacechem.1c00296
ACS Earth Space Chem. 2021, 5, 3458−3473

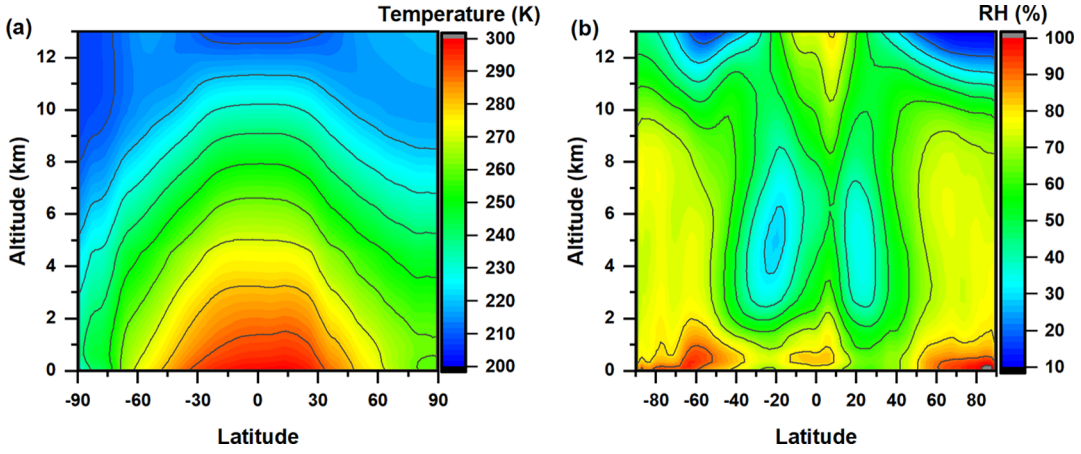

Figure 2. Altitude profiles for (a) temperature and (b) RH as a function of latitude calculated using the EMAC model for the years 2005 to 2009.

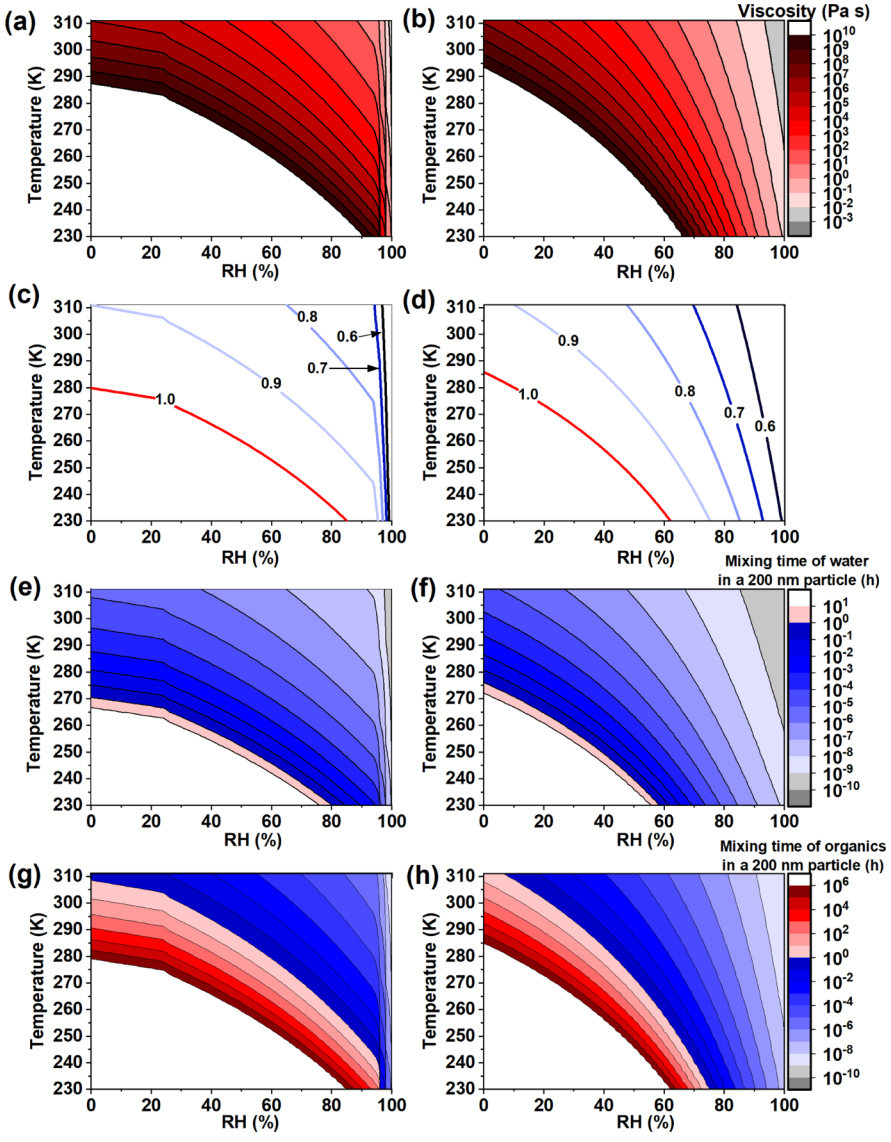

Figure 3. Properties of simulated pine tree SOA and toluene SOA as a function of temperature and RH. Panels (a,b) correspond to viscosity for (a) simulated pine tree SOA and (b) toluene SOA as a function of temperature and RH. Panels (c,d) correspond to T_g/T for (c) simulated pine tree SOA and (d) toluene SOA as a function of temperature and RH. Mixing times of water in a 200 nm particle are shown in panels (e,f) for (e) simulated pine tree SOA and (f) toluene SOA. Mixing times of organic molecules in a 200 nm particle are shown in panels (g,h) for (g) simulated pine tree SOA and (h) toluene SOA.

https://doi.org/10.1021/acsearthspacechem.1c00296
ACS Earth Space Chem. 2021, 5, 3458−3473

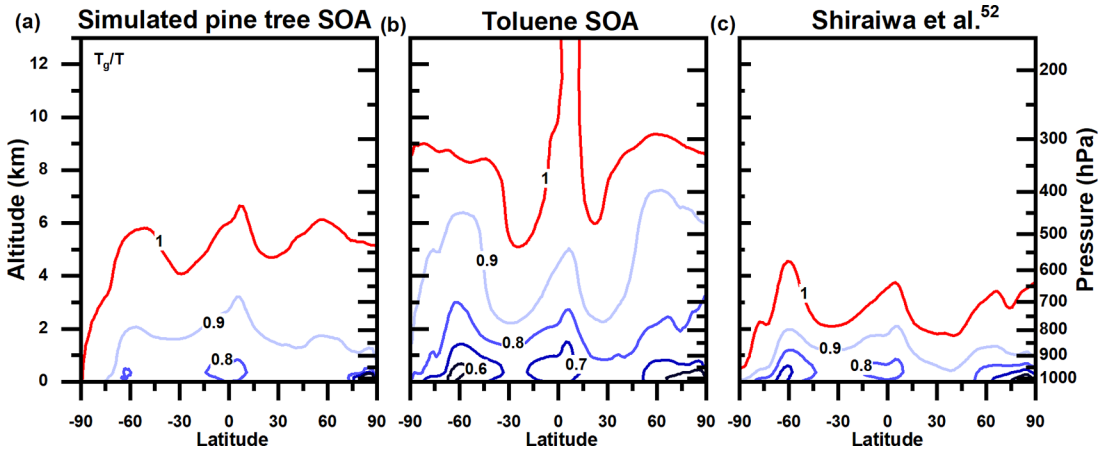

Figure 4. Annual average phase state of particles of (a) simulated pine tree SOA, (b) toluene SOA, and (c) SOA from Shiraiwa et al.[52] as a function of altitude and latitude. The particles are in the glassy state when $T_g/T \geq 1$. The red contour line corresponds to $T_g/T = 1$.

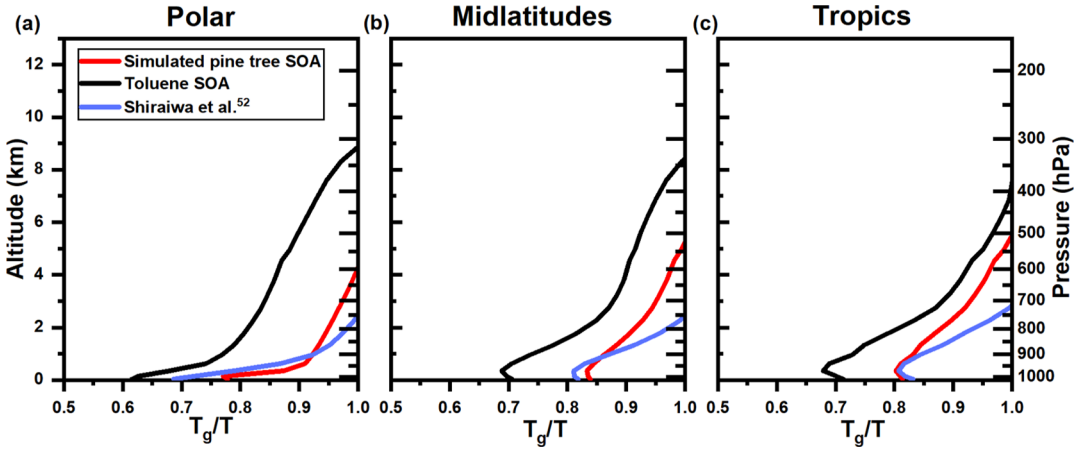

Figure 5. Annual average altitude profiles of T_g/T for (a) polar (latitude greater than 66.3° and less than −66.3°), (b) midlatitude (66.3 > latitude > 23.26° and −66.3 < latitude < −23.26°), and (c) tropical (23.26 > latitude > −23.26°) regions for simulated pine tree SOA (red), toluene SOA (black), and SOA from Shiraiwa et al.[52] (blue).

approach was their predictions corresponded to the total SOA (biogenic and anthropogenic SOA combined) rather than biogenic and anthropogenic SOA separately, although it should be kept in mind that on a global scale, biogenic SOA dominates over anthropogenic SOA. Shiraiwa et al.[52] mostly focused on results from three atmospheric pressures: surface pressure, 850 and 500 hPa. Here, for comparison purposes, the predictions from Shiraiwa et al.[52] are replotted as a function of latitude and altitude. As mentioned above, their mixing times for organic molecules within SOA were increased by a factor of 4 to be consistent with the radius of the organic diffusing molecule used in our study.

2.5. RH and Temperature in the Troposphere. Information on the RH and temperature in the troposphere is needed to assess the phase of SOA and the mixing times within the particles. Average annual RH and temperature fields were calculated using the model EMAC for the years 2005 to 2009. The same RH and temperature fields were used by Shiraiwa et al.[52] RH and temperature were determined as functions of pressure, latitude, and longitude. From the pressure, the altitude (h) was calculated using eq 12[98]

$$h = \frac{1 - \left(\frac{P}{P_0}\right)^{R\lambda/gM_{air}}}{\frac{\lambda}{T_0}} \quad (12)$$

where P_0 is the pressure at sea level (101 325 Pa), P is the pressure at the altitude being calculated, R is the gas constant (8.3145 J mol^{-1} K^{-1}), λ is the temperature lapse rate (6.5 K km^{-1}), g is the standard gravity (9.806 m s^{-2}), M_{air} is the molecular mass of air (28.97 g mol^{-1}), and T_0 is the temperature at the surface (288.15 K). Temperature and RH values were averaged across longitude to give values as a function of latitude and altitude (Figure 2).

3. RESULTS AND DISCUSSION

3.1. Parameterization of the Viscosity, T_g/T, and Mixing Times of SOA Particles as a Function of Temperature and RH. Shown in Figure 3 are the parameterizations of viscosity, T_g/T, and mixing times as a function of RH and temperature developed using the procedures described above. Here we highlight a few points: (1) As expected, the viscosity depends strongly on RH and temperature, with the viscosity increasing as the RH and temperature decrease (Figure 3a,b). An increase in viscosity with a decrease in RH is expected since water is a plasticizer,

https://doi.org/10.1021/acsearthspacechem.1c00296
ACS Earth Space Chem. 2021, 5, 3458−3473

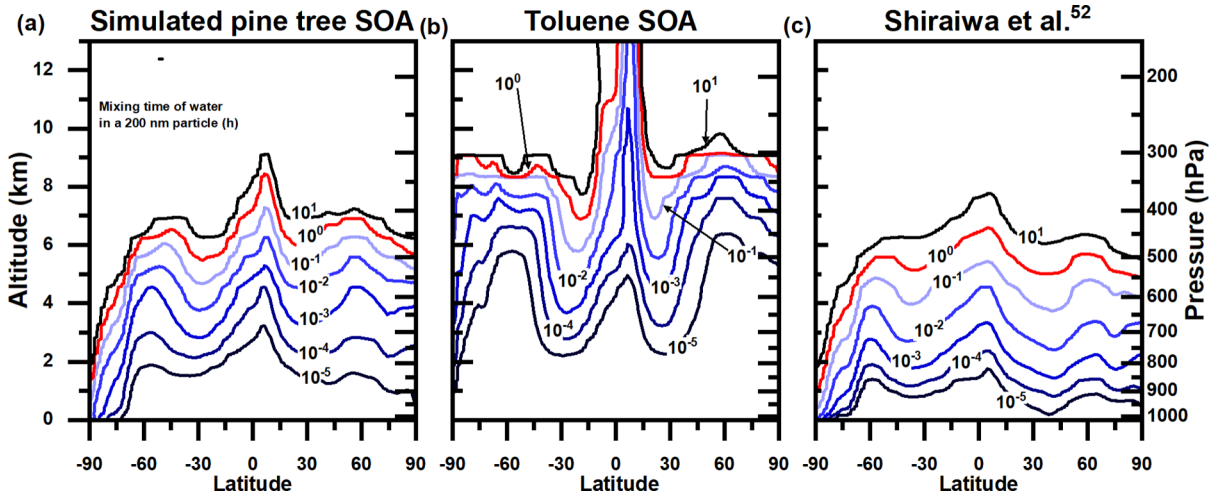

Figure 6. Annual average mixing time of water in a 200 nm particle for (a) simulated pine tree SOA, (b) toluene SOA, and (c) SOA from Shiraiwa et al.[52] as a function of altitude and latitude. The contour lines correspond to mixing times in hours. The red contour line corresponds to a mixing time of 1 h.

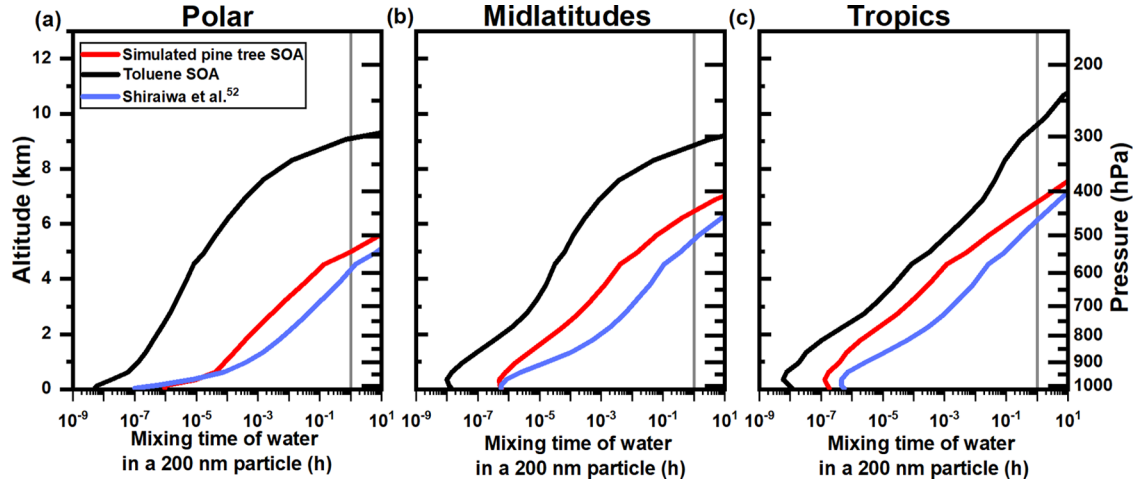

Figure 7. Annual average altitude profiles of the mixing time of water in a 200 nm particle for (a) polar (latitude greater than 66.3° and less than −66.3°), (b) midlatitude (66.3 > latitude > 23.26° and −66.3 < latitude < −23.26°), and (c) tropical (23.26 > latitude > −23.26°) regions for simulated pine tree SOA (red), toluene SOA (black), and SOA from Shiraiwa et al.[52] (blue). The vertical lines are included to highlight a mixing time of 1 h. Average mixing time values were calculated using the average of the log mixing time data as a function of latitude.

and a decrease in RH leads to a decrease in the water content of the SOA. An increase in viscosity with a decrease in temperature is expected since viscous flow is an activated process. (2) At RH = 0%, the simulated pine tree SOA and toluene SOA are in a glassy state at temperatures ≤280 and ≤285 K, respectively (Figure 3c,d). This illustrates that SOA can be in a glassy state at temperatures approaching room temperature if RH is very low, though such conditions are not commonly expected in the atmosphere. However, it should be kept in mind that the glass transition temperature is highly dependent on RH. For example, at RH = 60%, the simulated pine tree SOA and toluene SOA do not reach the glassy state until the temperature is ≤250 and ≤235 K, respectively. (3) At the same RH and temperature, the mixing times of organics are much longer than the mixing times of water within the same type of SOA. For example, at 0% RH and 280 K, the mixing times of organics are at least a factor of 10^8 longer than the mixing times of water within the simulated pine tree SOA (Figure 3e,g). This is because small molecules, such as water, can more easily diffuse through SOA particles than larger organic molecules.

3.2. Global Distributions of the Glassy State. Shown in Figure 4 are predicted annual average T_g/T values as a function of altitude and latitude for simulated pine tree SOA (Figure 4a) and toluene SOA (Figure 4b). As mentioned above, SOA is in a glassy phase state when $T_g/T \geq 1$. The altitude above which SOA was expected to vitrify was in the FT region and depended on the latitude. To better illustrate the latitudinal dependence, Figure 5 shows the annual average T_g/T values as a function of altitude for the tropical regions (−23.26 to 23.26°), midlatitude regions (−23.26 to −66.3° and 23.26 to 66.3°), and polar regions (less than −66.3° and greater than 66.3°). The patterns of T_g/T as a function of altitude and latitude were similar in the northern and southern hemispheres (Figure 4) since the patterns of RH and temperature as a function of altitude and latitude were similar in both hemispheres (Figure 2). In addition, the shape of the T_g/T = 1 isopleth for simulated pine tree SOA was similar to that of toluene SOA, except the T_g/T = 1 isopleth for toluene SOA

https://doi.org/10.1021/acsearthspacechem.1c00296
ACS Earth Space Chem. 2021, 5, 3458−3473

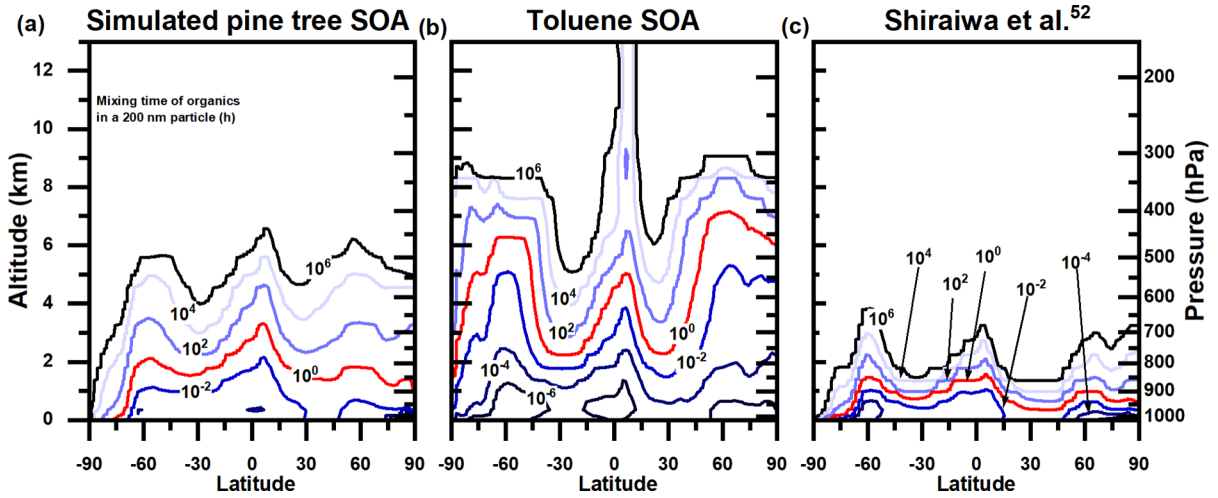

Figure 8. Annual average mixing time of organic molecules within SOA for (a) simulated pine tree SOA, (b) toluene SOA, and (c) SOA from Shiraiwa et al.[52] as a function of altitude and latitude. The contour lines correspond to mixing times in hours. The red contour line corresponds to a mixing time of 1 h.

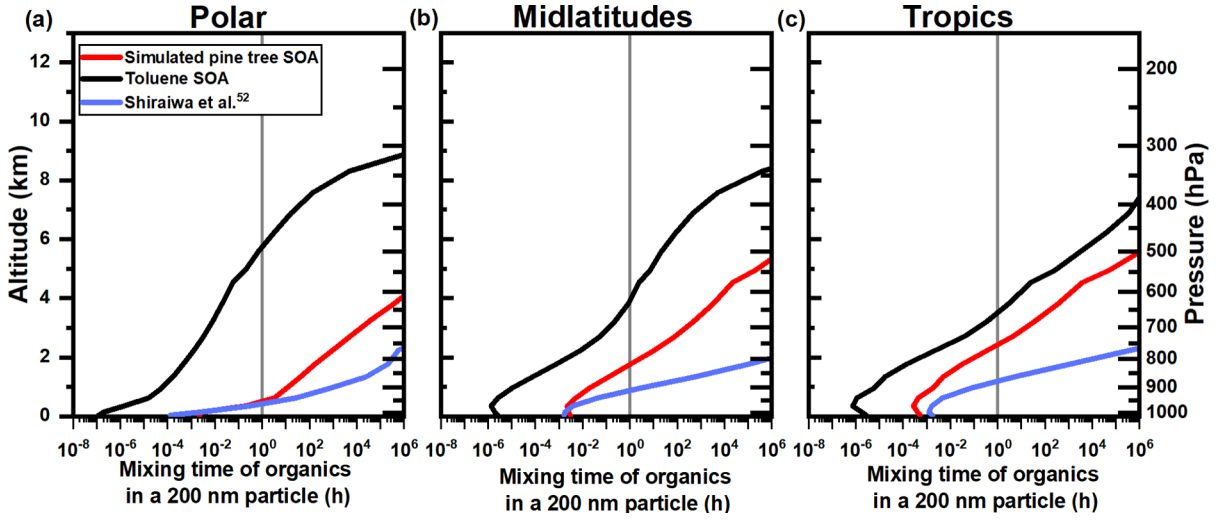

Figure 9. Annual average altitude profiles of the mixing time of organics in a 200 nm particle for (a) polar (latitude greater than 66.3° and less than −66.3°), (b) midlatitude (66.3 > latitude > 23.26° and −66.3 < latitude < −23.26°), and (c) tropical (23.26 > latitude > −23.26°) regions for simulated pine tree SOA (red), toluene SOA (black), and SOA from Shiraiwa et al.[52] (blue). The vertical lines are included to highlight a mixing time of 1 h. Average mixing time values were calculated using the average of the log mixing time data as a function of latitude.

occurred at 1−2 km higher in altitude. Based on Figure 4, the lowest altitude at which the glassy state was observed was 0 km for simulated pine tree SOA and 5 km for toluene SOA, occurring at a latitude of −90 and −30°, respectively. The glassy state should be rare in the PBL based on these predictions.

The glassy phase state first occurs at a latitude of −90° but not 90° for the simulated pine tree SOA due to the difference in temperatures. At a latitude of −90°, the temperature was ∼30 K lower than the temperature at 90°, resulting in higher viscosities.

For simulated pine tree SOA in the polar, midlatitude, and tropical regions, the annual average T_g/T could exceed 1, indicating the formation of a glassy state at altitudes of 4.25, 5.25, and 5.5 km, respectively (Figure 5). For toluene SOA in the polar, midlatitude, and tropical regions, the average T_g/T could exceed 1 at altitudes of 8.75, 8.5, and 7.25 km, respectively (Figure 5).

The results from Shiraiwa et al.[52] are shown in Figures 4c and 5 for comparison. As discussed above, their results corresponded to combined biogenic and anthropogenic SOA. However, biogenic sources dominate outside urban environments and in the FT since anthropogenic sources only contribute approximately 10% to the total SOA budget.[2,99] The predictions from Shiraiwa et al.[52] had a similar shape to the results for simulated pine tree SOA and toluene SOA (Figure 4c), except the $T_g/T = 1$ isopleth was shifted to lower altitudes. The $T_g/T = 1$ isopleth from Shiraiwa et al.[52] was approximately 1−4 km lower in altitude than the simulated pine tree SOA predictions depending on the latitude. At a latitude of −90°, the lowest altitude at which the glassy state might be observed is 0.5 km based on the results from Shiraiwa et al.[52] For the polar, midlatitude, and tropical regions, the average T_g/T might exceed 1 at altitudes of 2.5, 2.5, and 3 km, respectively, based on Shiraiwa et al.[52] The glassy state was also rare in the PBL, except over dry lands based on the Shiraiwa et al.[52] predictions.

https://doi.org/10.1021/acsearthspacechem.1c00296
ACS Earth Space Chem. 2021, 5, 3458−3473

3.3. Global Distributions of Water Mixing Times. Shown in Figures 6 and 7 are the predicted global distributions of the annual average mixing times of water in 200 nm particles. The shape of the 1 h isopleth for simulated pine tree SOA was similar to that of the 1 h isopleth for toluene SOA, except the toluene SOA 1 h isopleth occurred 2−3 km higher in altitude. Based on Figure 6, the lowest altitude where the mixing times of water were greater than or equal to 1 h was 1.5 km for simulated pine tree SOA and 8 km for toluene SOA occurring at latitudes of −90 and −30°, respectively. The mixing time of water reached 1 h for the simulated pine tree SOA at a latitude of −90°, but not 90°, due to the lower temperatures at −90° compared to 90°, as discussed above. For simulated pine tree SOA in the polar, midlatitude, and tropical regions, the average mixing time of water was greater than or equal to 1 h at altitudes of 5, 6.5, and 6.75 km, respectively (Figure 7). For toluene SOA in the polar, midlatitude, and tropical regions, the average mixing time of water was greater than or equal to 1 h at altitudes of 9, 8.75, and 9.5 km, respectively (Figure 7).

The results from Shiraiwa et al.[52] had a similar shape to the simulated pine tree SOA and toluene SOA results (Figure 6c), except that the 1 h isopleth was at lower altitudes. At a latitude of −90° (Figure 6c), Shiraiwa et al.[52] predicted the mixing time of water to be greater than 1 h at altitudes of 1 km. The average mixing time of water in polar, midlatitude, and tropical regions could be greater than 1 h at altitudes of 4.5, 5.5, and 6 km, respectively (Figure 7).

3.4. Global Distributions of Organic Mixing Times. Shown in Figures 8 and 9 are the predicted global distributions of annual average mixing times of organic molecules in 200 nm particles. The lowest altitude at which the mixing times of organics exceeded 1 h was 0 km for simulated pine tree SOA (Figure 8a) and 1.5 km for toluene SOA (Figure 8b) corresponding to −90° latitude. The mixing times of organics were less than 1 h in the PBL based on both the simulated pine tree and toluene SOA predictions.

Simulated pine tree SOA in the polar, midlatitude, and tropical regions could have an average mixing time of organics ≥1 h at altitudes of 0.5, 1.75, and 2.5 km, respectively (Figure 9). Toluene SOA in the polar, midlatitude, and tropical regions could have an average organic mixing time ≥1 h at altitudes of 5.75, 4, and 3.5 km, respectively (Figure 9).

Similar to T_g/T and the water mixing times, the results for the mixing time of organics by Shiraiwa et al.[52] had a shape similar to the simulated pine tree and toluene SOA results (Figure 8c), except the 1 h isopleth occurred at a lower altitude. At a latitude of −90° (Figure 8c), the mixing time of organics could exceed 1 h at the surface. The average mixing times of organics in the polar, midlatitude, and tropical regions could be greater than 1 h at altitudes of 0.5, 1, and 1 km, respectively (Figure 9). The mixing times of organics were often less than 1 h in the PBL based on the Shiraiwa et al.[52] predictions.

In our analysis, we focused on a mixing time of 1 h. Typical timescales used in global atmospheric models are often in the range of 0.5−1 h. The overall conclusions reached here do not change if a timescale of 0.5 h is used instead of 1 h (Figures S1 and S2).

3.5. Possible Reasons for the Difference between the Current Results and Shiraiwa et al. The T_g/T values, mixing times of water, and mixing times of organics predicted by Shiraiwa et al.[52] were greater than those predicted here for the same altitude and latitude. These differences could be due to several reasons. For example, the method used to predict viscosities by Shiraiwa et al.[52] was very different than the method used here (see Section 2.4 for details). Several parameters were needed for the predictions by Shiraiwa et al.[52] including the hygroscopicity and Gordon−Taylor constants for the SOA. These parameters each have their own uncertainties, which could lead to an under or over prediction of the viscosity of the SOA. In addition, the parameterization used by Shiraiwa et al.[52] to convert molar mass and O/C to a glass transition temperature had an uncertainty of ±15 K for individual components, which could also lead to an under or over prediction of the viscosity of the SOA at a given temperature and RH, although the uncertainty might be as small as ±3 K for SOA mixtures.

In our study, we used experimentally determined viscosity measurements of SOA generated in an environmental chamber. In this case, the SOA was formed during a short time period (less than 2 h) and hence corresponded to fresh SOA. In contrast, the simulations by Shiraiwa et al.[52] took into account atmospheric aging of fresh SOA using a chemistry-climate model. This atmospheric aging could lead to reduced volatilities and higher viscosities, T_g/T values, and mixing times.[46,100−105] In addition, the SOA used to generate the parameterization for the simulated pine tree SOA discussed here was produced with mass concentrations of 50−60 $\mu g\ m^{-3}$,[58] which was higher than SOA mass concentrations found in the FT. Previous studies have shown that higher mass concentrations could lead to lower viscosities and hence lower T_g/T values and mixing times.[36,103,106] In contrast, Shiraiwa et al.[52] used a chemical transport model to predict mass concentrations, which was able to reproduce spatial distributions and mass concentrations of SOA measured in the troposphere.[107] The SOA used to generate the parameterization for toluene SOA was produced with mass concentrations of either 60−100 or 600−1000 $\mu g\ m^{-3}$, with no dependence of the viscosity on the production mass concentration.[48] As a result, it is unknown whether the viscosity would increase at lower mass concentrations for the toluene SOA.

As a proxy of biogenic SOA, we used SOA generated from a mixture of VOCs representative of tree emissions. It is expected that this SOA would be a good proxy for SOA over a boreal forest.[58,61,62] However, it might not be a good proxy for biogenic SOA over all types of biomes because the composition of emitted VOCs varies greatly between different plant functional types.[108] The results from Shiraiwa et al.[52] included emissions from both boreal and temperate forests, which could produce differing results in regions with temperate forests.

Finally, Shiraiwa et al.[52] took into account various emission of VOCs from both anthropogenic and biogenic sources. Conversely, we used a single VOC (toluene) to represent anthropogenic emissions and a mixture of VOCs similar to emissions of VOCs from pine trees to represent biogenic SOA. Differences in the VOCs used to generate SOA in our experiments and the model by Shiraiwa et al.[52] could also lead to differences in viscosities. For example, SOA generated from the photooxidation of isoprene and SOA generated from the ozonolysis of α-pinene gave different viscosities than SOA from pine tree emissions.[36,58,109] As a result, the predicted viscosities from either study would be dependent on the

https://doi.org/10.1021/acsearthspacechem.1c00296
ACS Earth Space Chem. 2021, 5, 3458−3473

Table 1. Altitudes at Which SOA Reaches a Glassy State and Mixing Time of Water and Organics in SOA Are Greater Than 1 h for Different Regions of the Earth[a]

		region of the earth				
SOA property	source of SOA	−90° latitude (km)	−30° latitude (km)	tropical (km)	midlatitude (km)	polar (km)
T_g/T greater than 1	simulated pine tree SOA (current study)	0	4	5.5	5.25	4.25
	Shiraiwa et al.[52] (mostly biogenic SOA)	0.5	2	3	2.5	2.5
	toluene SOA (current study)	8.5	5	7.25	8.5	8.75
mixing time of water greater than 1 h in 200 nm SOA	Simulated pine tree SOA (current study)	1.5	5.5	6.75	6.5	5
	Shiraiwa et al.[52] (mostly biogenic SOA)	1	5	6	5.5	4.5
	toluene SOA (current study)	8.5	8	9.5	8.75	9
mixing time of organics greater than 1 h in 200 nm SOA	simulated pine tree SOA (current study)	0	1.5	2.5	1.75	0.5
	Shiraiwa et al.[52] (mostly biogenic SOA)	0	0.75	1	1	0.5
	toluene SOA (current study)	1.5	2.25	3.5	4	5.75

[a]Latitudes of −90 and −30° are shown since these latitudes correspond to the lowest altitudes that SOA reaches a glassy state, and the mixing times of water and organics in SOA are greater than 1 h for simulated pine tree SOA and toluene SOA, respectively.

precursor VOCs used for the SOA, potentially causing different predictions of viscosity.

In conclusion, the differences between the current study and the study by Shiraiwa et al.[52] might be explained by the higher mass concentrations and lack of chemical aging of the SOA used to develop the pine tree SOA parameterization, as well as the VOCs that contributed to the SOA in each study. The differences in methodologies used to predict viscosity might also play a role.

4. SUMMARY, CONCLUSIONS, IMPLICATIONS, AND OUTLOOK

Parameterizations for viscosity as a function of temperature and RH were developed for simulated pine tree SOA (biogenic SOA proxy) and toluene SOA (anthropogenic SOA proxy) based on room-temperature viscosity data. Based on these parameterizations, as well as tropospheric RH and temperature fields, the phase state and mixing times of water and organic molecules in SOA particles were predicted. Some of the key results are summarized and compared with Shiraiwa et al.[52] in Table 1. Based on our results, the glassy state can often occur, and the mixing time of water can often exceed 1 h at altitudes >6 km. The mixing time of organic molecules can often exceed 1 h throughout most of the FT. The glassy state is not important in the PBL and the mixing time of water and organic molecules is less than 1 h for most of the PBL. The latter conclusion is consistent with previous predictions, field measurements, and laboratory studies of SOA at temperatures and RH values common for the PBL.[43,50,110−114]

The timescale of a typical updraft in the atmosphere is between a few minutes and 1 h.[16] During an updraft, the temperature will decrease and the RH will increase. Due to the long mixing times of water in SOA at altitudes >6 km, SOA may not be able to reach equilibrium with the surrounding RH during updrafts in this region of the atmosphere. As a result, heterogenous ice nucleation by the glassy state will be more likely since a glassy core is more likely to be able to persist during an updraft in this region of the atmosphere.

Long mixing times of organics in the FT have implications for the long-range transport of pollutants such as polycyclic aromatic hydrocarbons. Previous studies have shown that aerosol particles can undergo long-range transport at altitudes of 2−6 km depending on the latitude and longitude.[115−117] These altitudes correspond to altitudes where the mixing times of organics within SOA can be long. As a result, pollutant molecules can be trapped within SOA particles during long-range transport, inhibiting their degradation via oxidation.[34,118−121]

The mixing time of organics in SOA is predicted to be less than 1 h for most of the PBL, where the majority of SOA is formed. This means that the assumption of equilibrium partitioning for SOA formation used in global chemical transport models is reasonable for most of the PBL, consistent with previous conclusions.[43,50,52,112,119−121] Equilibrium partitioning for SOA may not be valid in cases where SOA is formed in the FT.[122]

Our results are qualitatively consistent with the findings in Shiraiwa et al.,[52] but there are quantitative differences. The T_g/T values, mixing times of water, and mixing times of organics predicted by Shiraiwa et al.[52] were larger than those predicted here for the same altitude and latitude. In addition, the glassy state was predicted to occur at roughly 2 km lower in altitude by Shiraiwa et al.[52] Furthermore, mixing times of organic molecules within SOA were predicted to exceed 1 h at approximately 1 km lower in altitude by Shiraiwa et al.[52] Additional studies are needed to better understand the reasons for these differences.

Both this study and the study by Shiraiwa et al.[52] investigated mixing times within SOA particles with diameters of 200 nm. These calculations could be extended to other particles sizes, and the results would scale as the diameter squared. As a result, larger particles would have longer mixing times and smaller particles would have shorter mixing times. The phase state calculations (i.e., T_g/T values) are independent of the particle size so the predications presented by both studies would apply to all SOA particles in the accumulation mode.

For biogenic SOA, this study focused on simulated healthy pine tree SOA, where the VOC emissions are predominately monoterpenes with a small contribution from sesquiterpenes.[66] However, it has been shown that the VOC emission profile can

https://doi.org/10.1021/acsearthspacechem.1c00296
ACS Earth Space Chem. 2021, 5, 3458−3473

change when the tree is stressed,[60,66] and the prevalence of plant stress conditions is increasing in frequency and severity.[123−125] The SOA generated from the stress trees has been shown to have a higher viscosity than the healthy trees,[58] meaning that the prevalence of glassy SOA from pine trees could increase in the future.

The biogenic and anthropogenic SOA were considered separately in the current study, whereas SOA in the atmosphere would likely be a mixture of SOA from multiple biogenic sources and anthropogenic sources. To apply the method described in the current study to mixtures, mixing rules for viscosities could be used.[42,126−128] These mixing rules have been used in the past to predict the viscosity of organic−water and SOA−water mixtures with some success.

To improve predictions of phase state, mixing times of water, and mixing times of organic molecules in SOA particles, laboratory viscosity or diffusion measurements as a function of RH are needed for SOA prepared at lower, more atmospherically relevant mass concentrations. Explicit measurements of viscosity at reduced temperatures are needed as well. In addition, viscosity or diffusion measurements of more oxidized (i.e., aged) SOA are needed to better replicate atmospheric SOA. The current study used simulated pine tree SOA and toluene SOA to represent biogenic SOA and anthropogenic SOA, respectively. Similar studies with other types of SOA are also needed. These experiments will provide a greater understanding of the phase state and mixing times in atmospheric SOA, which will allow for improved predictions of these properties. Other important types of SOA include biomass burning SOA and low volatility isoprene-derived epoxydiols (IEPOX)-SOA.[129,130] Although viscosities of primary biomass burning organic aerosol have been estimated based on chemical composition or volatility distributions,[70,105] viscosities of SOA from biomass burning have not been reported in the literature. IEPOX-SOA has been shown to have relatively high viscosity,[129,130] similar or higher than that of the simulated pine tree SOA discussed here.

Similar to Shiraiwa et al.,[52] the results presented here are based on average annual RH and temperature fields. Additional studies are needed to determine how the global distributions of the phase state and mixing times within SOA change with the time of day and season. The RH and temperature fields in the FT will depend less on the time of the day than at the surface.[131,132] In the PBL, RH and temperature will vary significantly with the time of day and season, and hence the phase state and mixing times within SOA are also expected to vary with the time of day and season.[54,133−135]

■ ASSOCIATED CONTENT

Supporting Information

The Supporting Information is available free of charge at https://pubs.acs.org/doi/10.1021/acsearthspacechem.1c00296.

Viscosity measurements using poke-flow; viscosity measurements using FRAP; activity-based mixing rule derivation; and viscosity of water as a function of temperature calculation (PDF)

■ AUTHOR INFORMATION

Corresponding Author

Allan K. Bertram − *Department of Chemistry, University of British Columbia, Vancouver, British Columbia V6T 1Z1, Canada;* orcid.org/0000-0002-5621-2323; Email: bertram@chem.ubc.ca

Authors

Adrian M. Maclean − *Department of Chemistry, University of British Columbia, Vancouver, British Columbia V6T 1Z1, Canada;* orcid.org/0000-0003-0901-5287

Ying Li − *Department of Chemistry, University of California Irvine, Irvine, California 92697, United States;* Present Address: Institute of Atmospheric Physics, Chinese Academy of Sciences, Beijing, 100029, China

Giuseppe V. Crescenzo − *Department of Chemistry, University of British Columbia, Vancouver, British Columbia V6T 1Z1, Canada;* orcid.org/0000-0003-0936-3935

Natalie R. Smith − *Department of Chemistry, University of California Irvine, Irvine, California 92697, United States*

Vlassis A. Karydis − *Institute of Energy & Climate Research, IEK-8: Troposphere, Forschungszentrum Jülich GmbH, 52428 Jülich, Germany*

Alexandra P. Tsimpidi − *Institute of Energy & Climate Research, IEK-8: Troposphere, Forschungszentrum Jülich GmbH, 52428 Jülich, Germany; Institute for Environmental Research & Sustainable Development, National Observatory of Athens, 15236 Palea Penteli, Greece*

Christopher L. Butenhoff − *Dept. of Physics, Portland State University, Portland, Oregon 97201, United States*

Celia L. Faiola − *Department of Chemistry and Department of Ecology and Evolutionary Biology, University of California Irvine, Irvine, California 92697, United States;* orcid.org/0000-0002-4987-023X

Jos Lelieveld − *Atmospheric Chemistry Department, Max Planck Institute for Chemistry, 55128 Mainz, Germany; Climate and Atmosphere Research Center, The Cyprus Institute, 1645 Nicosia, Cyprus;* orcid.org/0000-0001-6307-3846

Sergey A. Nizkorodov − *Department of Chemistry, University of California Irvine, Irvine, California 92697, United States;* orcid.org/0000-0003-0891-0052

Manabu Shiraiwa − *Department of Chemistry, University of California Irvine, Irvine, California 92697, United States;* orcid.org/0000-0003-2532-5373

Complete contact information is available at: https://pubs.acs.org/10.1021/acsearthspacechem.1c00296

Notes

The authors declare no competing financial interest.

■ ACKNOWLEDGMENTS

We thank Alexander Laskin, Anusha P. S. Hettiyadura, and Kyla Siemens for their work collecting the mass spectrum of the healthy tree SOA. We thank Jose Jimenez for very helpful discussions during the initial stages of this research. The UBC team was funded by the Natural Science and Engineering Research Council of Canada. N.R.S. thanks the University of California, Irvine Department of Chemistry for support with Rowland Graduate Research Fellowship and US National Science Foundation (grant AGS-1853639). M.S. thanks the National Science Foundation (AGS-1654104) and the Department of Energy (DE-SC0018349 and DE-SC0022139) for funding.

REFERENCES

(1) Ervens, B.; Turpin, B. J.; Weber, R. J. Secondary Organic Aerosol Formation in Cloud Droplets and Aqueous Particles (AqSOA): A Review of Laboratory, Field and Model Studies. *Atmos. Chem. Phys.* **2011**, *11*, 11069−11102.

(2) Hallquist, M.; Wenger, J. C.; Baltensperger, U.; Rudich, Y.; Simpson, D.; Claeys, M.; Dommen, J.; Donahue, N. M.; George, C.; Goldstein, A. H.; Hamilton, J. F.; Herrmann, H.; Hoffmann, T.; Iinuma, Y.; Jang, M.; Jenkin, M. E.; Jimenez, J. L.; Kiendler-Scharr, A.; Maenhaut, W.; McFiggans, G.; Mentel, T. F.; Monod, A.; Prévôt, A. S. H.; Seinfeld, J. H.; Surratt, J. D.; Szmigielski, R.; Wildt, J. The Formation, Properties and Impact of Secondary Organic Aerosol: Current and Emerging Issues. *Atmos. Chem. Phys.* **2009**, *9*, 5155−5236.

(3) *IPCC 2013: Climate Change 2013: The Physical Science Basis. Contribution of Working Group I to the Fifth Assessment Report of the Intergovernmental Panel on Climate Change*; Stocker, T. F., Quin, D., Plattner, G.-K., Tignor, M. M. B., Allen, S. K., Boschung, J., Nauels, A., Xia, Y., Bex, V., Midgley, P. M., Eds.; Cambridge University Press: Cambridge, U.K., 2013.

(4) Shiraiwa, M.; Ueda, K.; Pozzer, A.; Lammel, G.; Kampf, C. J.; Fushimi, A.; Enami, S.; Arangio, A. M.; Fröhlich-Nowoisky, J.; Fujitani, Y.; Furuyama, A.; Lakey, P. S. J.; Lelieveld, J.; Lucas, K.; Morino, Y.; Pöschl, U.; Takahama, S.; Takami, A.; Tong, H.; Weber, B.; Yoshino, A.; Sato, K. Aerosol Health Effects from Molecular to Global Scales. *Environ. Sci. Technol.* **2017**, *51*, 13545−13567.

(5) Pope, C. A., III; Dockery, D. D. Health Effects of Fine Particulate Air Pollution: Lines That Connect. *J. Air Waste Manage. Assoc.* **2006**, *56*, 709−742.

(6) Lelieveld, J.; Evans, J. S.; Fnais, M.; Giannadaki, D.; Pozzer, A. The Contribution of Outdoor Air Pollution Sources to Premature Mortality on a Global Scale. *Nature* **2015**, *525*, 367−371.

(7) Cohen, A. J.; Brauer, M.; Burnett, R.; Anderson, H. R.; Frostad, J.; Estep, K.; Balakrishnan, K.; Brunekreef, B.; Dandona, L.; Dandona, R.; Feigin, V.; Freedman, G.; Hubbell, B.; Jobling, A.; Kan, H.; Knibbs, L.; Liu, Y.; Martin, R.; Morawska, L.; Pope, C. A.; Shin, H.; Straif, K.; Shaddick, G.; Thomas, M.; van Dingenen, R.; van Donkelaar, A.; Vos, T.; Murray, C. J. L.; Forouzanfar, M. H. Estimates and 25-Year Trends of the Global Burden of Disease Attributable to Ambient Air Pollution: An Analysis of Data from the Global Burden of Diseases Study 2015. *Lancet* **2017**, *389*, 1907−1918.

(8) Lelieveld, J. Clean Air in the Anthropocene. *Faraday Discuss.* **2017**, *200*, 693−703.

(9) Koop, T.; Bookhold, J.; Shiraiwa, M.; Pöschl, U. Glass Transition and Phase State of Organic Compounds: Dependency on Molecular Properties and Implications for Secondary Organic Aerosols in the Atmosphere. *Phys. Chem. Chem. Phys.* **2011**, *13*, 19238−19255.

(10) Ignatius, K.; Kristensen, T. B.; Järvinen, E.; Nichman, L.; Fuchs, C.; Gordon, H.; Herenz, P.; Hoyle, C. R.; Duplissy, J.; Garimella, S.; Dias, A.; Frege, C.; Höppel, N.; Tröstl, J.; Wagner, R.; Yan, C.; Amorim, A.; Baltensperger, U.; Curtius, J.; Donahue, N. M.; Gallagher, M. W.; Kirkby, J.; Kulmala, M.; Möhler, O.; Saathoff, H.; Schnaiter, M.; Tomé, A.; Virtanen, A.; Worsnop, D.; Stratmann, F. Heterogeneous Ice Nucleation of Viscous Secondary Organic Aerosol Produced from Ozonolysis of α-Pinene. *Atmos. Chem. Phys.* **2016**, *16*, 6495−6509.

(11) Murray, B. J.; Wilson, T. W.; Dobbie, S.; Cui, Z.; Al-Jumur, S. M. R. K.; Möhler, O.; Schnaiter, M.; Wagner, R.; Benz, S.; Niemand, M.; Saathoff, H.; Ebert, V.; Wagner, S.; Kärcher, B. Heterogeneous Nucleation of Ice Particles on Glassy Aerosols under Cirrus Conditions. *Nat. Geosci.* **2010**, *3*, 233−237.

(12) Wagner, R.; Möhler, O.; Saathoff, H.; Schnaiter, M.; Skrotzki, J.; Leisner, T.; Wilson, T. W.; Malkin, T. L.; Murray, B. J. Ice Cloud Processing of Ultra-Viscous/Glassy Aerosol Particles Leads to Enhanced Ice Nucleation Ability. *Atmos. Chem. Phys.* **2012**, *12*, 8589−8610.

(13) Wang, B.; Lambe, A. T.; Massoli, P.; Onasch, T. B.; Davidovits, P.; Worsnop, D. R.; Knopf, D. A. The Deposition Ice Nucleation and Immersion Freezing Potential of Amorphous Secondary Organic Aerosol: Pathways for Ice and Mixed-Phase Cloud Formation. *J. Geophys. Res.* **2012**, *117*, D16209.

(14) Knopf, D. A.; Alpert, P. A.; Wang, B. The Role of Organic Aerosol in Atmospheric Ice Nucleation: A Review. *ACS Earth Space Chem.* **2018**, *2*, 168−202.

(15) Wolf, M. J.; Zhang, Y.; Zawadowicz, M. A.; Goodell, M.; Froyd, K.; Freney, E.; Sellegri, K.; Rösch, M.; Cui, T.; Winter, M.; Lacher, L.; Axisa, D.; DeMott, P. J.; Levin, E. J. T.; Gute, E.; Abbatt, J.; Koss, A.; Kroll, J. H.; Surratt, J. D.; Cziczo, D. J. A Biogenic Secondary Organic Aerosol Source of Cirrus Ice Nucleating Particles. *Nat. Commun.* **2020**, *11*, 4834.

(16) Berkemeier, T.; Shiraiwa, M.; Pöschl, U.; Koop, T. Competition between Water Uptake and Ice Nucleation by Glassy Organic Aerosol Particles. *Atmos. Chem. Phys.* **2014**, *14*, 12513−12531.

(17) Shiraiwa, M.; Seinfeld, J. H. Equilibration Timescale of Atmospheric Secondary Organic Aerosol Partitioning. *Geophys. Res. Lett.* **2012**, *39*, L24801.

(18) Zaveri, R. A.; Easter, R. C.; Shilling, J. E.; Seinfeld, J. H. Modeling Kinetic Partitioning of Secondary Organic Aerosol and Size Distribution Dynamics: Representing Effects of Volatility, Phase State, and Particle-Phase Reaction. *Atmos. Chem. Phys.* **2014**, *14*, 5153−5181.

(19) Zaveri, R. A.; Shilling, J. E.; Zelenyuk, A.; Liu, J.; Bell, D. M.; D'Ambro, E. L.; Gaston, C. J.; Thornton, J. A.; Laskin, A.; Lin, P.; Wilson, J.; Easter, R. C.; Wang, J.; Bertram, A. K.; Martin, S. T.; Seinfeld, J. H.; Worsnop, D. R. Growth Kinetics and Size Distribution Dynamics of Viscous Secondary Organic Aerosol. *Environ. Sci. Technol.* **2018**, *52*, 1191−1199.

(20) Shiraiwa, M.; Yee, L. D.; Schilling, K. A.; Loza, C. L.; Craven, J. S.; Zuend, A.; Ziemann, P. J.; Seinfeld, J. H. Size Distribution Dynamics Reveal Particle-Phase Chemistry in Organic Aerosol Formation. *Proc. Natl. Acad. Sci. U.S.A.* **2013**, *110*, 11746−11750.

(21) Kim, Y.; Sartelet, K.; Couvidat, F. Modeling the Effect of Non-Ideality, Dynamic Mass Transfer and Viscosity on SOA Formation in a 3-D Air Quality Model. *Atmos. Chem. Phys.* **2019**, *19*, 1241−1261.

(22) Yli-Juuti, T.; Pajunoja, A.; Tikkanen, O. P.; Buchholz, A.; Faiola, C.; Väisänen, O.; Hao, L.; Kari, E.; Peräkylä, O.; Garmash, O.; Shiraiwa, M.; Ehn, M.; Lehtinen, K.; Virtanen, A. Factors Controlling the Evaporation of Secondary Organic Aerosol from α-Pinene Ozonolysis. *Geophys. Res. Lett.* **2017**, *44*, 2562−2570.

(23) Zhang, Y.; Chen, Y.; Lambe, A. T.; Olson, N. E.; Lei, Z.; Craig, R. L.; Zhang, Z.; Gold, A.; Onasch, T. B.; Jayne, J. T.; Worsnop, D. R.; Gaston, C. J.; Thornton, J. A.; Vizuete, W.; Ault, A. P.; Surratt, J. D. Effect of the Aerosol-Phase State on Secondary Organic Aerosol Formation from the Reactive Uptake of Isoprene-Derived Epoxydiols (IEPOX). *Environ. Sci. Technol. Lett.* **2018**, *5*, 167−174.

(24) Steimer, S. S.; Lampimäki, M.; Coz, E.; Grzinic, G.; Ammann, M. The Influence of Physical State on Shikimic Acid Ozonolysis: A Case for in Situ Microspectroscopy. *Atmos. Chem. Phys.* **2014**, *14*, 10761−10772.

(25) Houle, F. A.; Hinsberg, W. D.; Wilson, K. R. Oxidation of a Model Alkane Aerosol by OH Radical: The Emergent Nature of Reactive Uptake. *Phys. Chem. Chem. Phys.* **2015**, *17*, 4412−4423.

(26) Liu, P.; Li, Y. J.; Wang, Y.; Bateman, A. P.; Zhang, Y.; Gong, Z.; Bertram, A. K.; Martin, S. T. Highly Viscous States Affect the Browning of Atmospheric Organic Particulate Matter. *ACS Cent. Sci.* **2018**, *4*, 207−215.

(27) Li, Z.; Smith, K. A.; Cappa, C. D. Influence of Relative Humidity on the Heterogeneous Oxidation of Secondary Organic Aerosol. *Atmos. Chem. Phys.* **2018**, *18*, 14585−14608.

(28) Hinks, M. L.; Brady, M. V.; Lignell, H.; Song, M.; Grayson, J. W.; Bertram, A. K.; Lin, P.; Laskin, A.; Laskin, J.; Nizkorodov, S. A. Effect of Viscosity on Photodegradation Rates in Complex Secondary Organic Aerosol Materials. *Phys. Chem. Chem. Phys.* **2016**, *18*, 8785−8793.

https://doi.org/10.1021/acsearthspacechem.1c00296
ACS Earth Space Chem. 2021, 5, 3458−3473

(29) Shiraiwa, M.; Ammann, M.; Koop, T.; Poschl, U. Gas Uptake and Chemical Aging of Semisolid Organic Aerosol Particles. *Proc. Natl. Acad. Sci. U.S.A.* **2011**, *108*, 11003−11008.
(30) Berkemeier, T.; Steimer, S. S.; Krieger, U. K.; Peter, T.; Pöschl, U.; Ammann, M.; Shiraiwa, M. Ozone Uptake on Glassy, Semi-Solid and Liquid Organic Matter and the Role of Reactive Oxygen Intermediates in Atmospheric Aerosol Chemistry. *Phys. Chem. Chem. Phys.* **2016**, *18*, 12662−12674.
(31) Li, Y. J.; Liu, P.; Gong, Z.; Wang, Y.; Bateman, A. P.; Bergoend, C.; Bertram, A. K.; Martin, S. T. Chemical Reactivity and Liquid/Nonliquid States of Secondary Organic Material. *Environ. Sci. Technol.* **2015**, *49*, 13264−13274.
(32) Li, J.; Forrester, S. M.; Knopf, D. A. Heterogeneous Oxidation of Amorphous Organic Aerosol Surrogates by O3, NO3, and OH at Typical Tropospheric Temperatures. *Atmos. Chem. Phys.* **2020**, *20*, 6055−6080.
(33) Zhao, Z.; Tolentino, R.; Lee, J.; Vuong, A.; Yang, X.; Zhang, H. Interfacial Dimerization by Organic Raical Reactions Uring Heterogeneous Oxiative Aging of Oxygenate Organic Aerosols. *J. Phys. Chem. A* **2019**, *123*, 10782−10792.
(34) Zhou, S.; Shiraiwa, M.; McWhinney, R. D.; Pöschl, U.; Abbatt, J. P. D. Kinetic Limitations in Gas-Particle Reactions Arising from Slow Diffusion in Secondary Organic Aerosol. *Faraday Discuss.* **2013**, *165*, 391−406.
(35) Abramson, E.; Imre, D.; Beránek, J.; Wilson, J.; Zelenyuk, A. Experimental Determination of Chemical Diffusion within Secondary Organic Aerosol Particles. *Phys. Chem. Chem. Phys.* **2013**, *15*, 2983−2991.
(36) Grayson, J. W.; Zhang, Y.; Mutzel, A.; Renbaum-Wolff, L.; Böge, O.; Kamal, S.; Herrmann, H.; Martin, S. T.; Bertram, A. K. Effect of Varying Experimental Conditions on the Viscosity of α-Pinene Derived Secondary Organic Material. *Atmos. Chem. Phys.* **2016**, *16*, 6027−6040.
(37) Kiland, K. J.; Maclean, A. M.; Kamal, S.; Bertram, A. K. Diffusion of Organic Molecules as a Function of Temperature in a Sucrose Matrix (a Proxy for Secondary Organic Aerosol). *J. Phys. Chem. Lett.* **2019**, *10*, 5902−5908.
(38) Evoy, E.; Kamal, S.; Patey, G. N.; Martin, S. T.; Bertram, A. K. Unified Description of Diffusion Coefficients from Small to Large Molecules in Organic-Water Mixtures. *J. Phys. Chem. A* **2020**, *124*, 2301−2308.
(39) Evoy, E.; Maclean, A. M.; Rovelli, G.; Li, Y.; Tsimpidi, A. P.; Karydis, V. A.; Kamal, S.; Lelieveld, J.; Shiraiwa, M.; Reid, J. P.; Bertram, A. K. Predictions of Diffusion Rates of Large Organic Molecules in Secondary Organic Aerosols Using the Stokes-Einstein and Fractional Stokes-Einstein Relations. *Atmos. Chem. Phys.* **2019**, *19*, 10073−10085.
(40) Bastelberger, S.; Krieger, U. K.; Luo, B.; Peter, T. Diffusivity Measurements of Volatile Organics in Levitated Viscous Aerosol Particles. *Atmos. Chem. Phys.* **2017**, *17*, 8453−8471.
(41) Reid, J. P.; Bertram, A. K.; Topping, D. O.; Laskin, A.; Martin, S. T.; Petters, M. D.; Pope, F. D.; Rovelli, G. The Viscosity of Atmospherically Relevant Organic Particles. *Nat. Commun.* **2018**, *9*, 956.
(42) Gervasi, N. R.; Topping, D. O.; Zuend, A. A Predictive Group-Contribution Model for the Viscosity of Aqueous Organic Aerosol. *Atmos. Chem. Phys.* **2020**, *20*, 2987−3008.
(43) Liu, P.; Li, Y. J.; Wang, Y.; Gilles, M. K.; Zaveri, R. A.; Bertram, A. K.; Martin, S. T. Lability of Secondary Organic Particulate Matter. *Proc. Natl. Acad. Sci. U.S.A.* **2016**, *113*, 12643−12648.
(44) Renbaum-Wolff, L.; Grayson, J. W.; Bateman, A. P.; Kuwata, M.; Sellier, M.; Murray, B. J.; Shilling, J. E.; Martin, S. T.; Bertram, A. K. Viscosity of α-Pinene Secondary Organic Material and Implications for Particle Growth and Reactivity. *Proc. Natl. Acad. Sci. U.S.A.* **2013**, *110*, 8014−8019.
(45) Zobrist, B.; Soonsin, V.; Luo, B. P.; Krieger, U. K.; Marcolli, C.; Peter, T.; Koop, T. Ultra-Slow Water Diffusion in Aqueous Sucrose Glasses. *Phys. Chem. Chem. Phys.* **2011**, *13*, 3514−3526.
(46) Zhang, Y.; Nichman, L.; Spencer, P.; Jung, J. I.; Lee, A.; Heffernan, B. K.; Gold, A.; Zhang, Z.; Chen, Y.; Canagaratna, M. R.; Jayne, J. T.; Worsnop, D. R.; Onasch, T. B.; Surratt, J. D.; Chandler, D.; Davidovits, P.; Kolb, C. E. The Cooling Rate- And Volatility-Dependent Glass-Forming Properties of Organic Aerosols Measured by Broadband Dielectric Spectroscopy. *Environ. Sci. Technol.* **2019**, *53*, 12366−12378.
(47) Li, Y.; Shiraiwa, M. Timescales of Secondary Organic Aerosols to Reach Equilibrium at Various Temperatures and Relative Humidities. *Atmos. Chem. Phys.* **2019**, *19*, 5959−5971.
(48) Song, M.; Liu, P. F.; Hanna, S. J.; Zaveri, R. A.; Potter, K.; You, Y.; Martin, S. T.; Bertram, A. K. Relative Humidity-Dependent Viscosity of Secondary Organic Material from Toluene Photo-Oxidation and Possible Implications for Organic Particulate Matter over Megacities. *Atmos. Chem. Phys.* **2016**, *16*, 8817−8830.
(49) Virtanen, A.; Joutsensaari, J.; Koop, T.; Kannosto, J.; Yli-Pirilä, P.; Leskinen, J.; Mäkelä, J. M.; Holopainen, J. K.; Pöschl, U.; Kulmala, M.; Worsnop, D. R.; Laaksonen, A. An Amorphous Solid State of Biogenic Secondary Organic Aerosol Particles. *Nature* **2010**, *467*, 824−827.
(50) Maclean, A. M.; Butenhoff, C. L.; Grayson, J. W.; Barsanti, K.; Jimenez, J. L.; Bertram, A. K. Mixing Times of Organic Molecules within Secondary Organic Aerosol Particles: A Global Planetary Boundary Layer Perspective. *Atmos. Chem. Phys.* **2017**, *17*, 13037−13048.
(51) Wallace, J. M.; Hobbs, P. V. *Atmospheric Science: An Introductory Survey*; Academic Press: Burlington, MA, 2006.
(52) Shiraiwa, M.; Li, Y.; Tsimpidi, A. P.; Karydis, V. A.; Berkemeier, T.; Pandis, S. N.; Lelieveld, J.; Koop, T.; Pöschl, U. Global Distribution of Particle Phase State in Atmospheric Secondary Organic Aerosols. *Nat. Commun.* **2017**, *8*, 15002.
(53) Schmedding, R.; Rasool, Q. Z.; Zhang, Y.; Pye, H. O. T.; Zhang, H.; Chen, Y.; Surratt, J. D.; Lopez-Hilfiker, F. D.; Thornton, J. A.; Goldstein, A. H.; Vizuete, W. Predicting Secondary Organic Aerosol Phase State and Viscosity and Its Effect on Multiphase Chemistry in a Regional-Scale Air Quality Model. *Atmos. Chem. Phys.* **2020**, *20*, 8201−8225.
(54) Li, Y.; Carlton, A. G.; Shiraiwa, M. Diurnal and Seasonal Variations in the Phase State of Secondary Organic Aerosol Material over the Contiguous US Simulated in CMAQ. *ACS Earth Space Chem.* **2021**, *5*, 1971−1982.
(55) Riipinen, I.; Pierce, J. R.; Yli-Juuti, T.; Nieminen, T.; Häkkinen, S.; Ehn, M.; Junninen, H.; Lehtipalo, K.; Petäjä, T.; Slowik, J.; Chang, R.; Shantz, N. C.; Abbatt, J.; Leaitch, W. R.; Kerminen, V.-M.; Worsnop, D. R.; Pandis, S. N.; Donahue, N. M.; Kulmala, M. Organic Condensation: A Vital Link Connecting Aerosol Formation to Cloud Condensation Nuclei (CCN) Concentrations. *Atmos. Chem. Phys.* **2011**, *11*, 3865−3878.
(56) Pöschl, U.; Martin, S. T.; Sinha, B.; Chen, Q.; Gunthe, S. S.; Huffman, J. A.; Borrmann, S.; Farmer, D. K.; Garland, R. M.; Helas, G.; Jimenez, J. L.; King, S. M.; Manzi, A.; Mikhailov, E.; Pauliquevis, T.; Petters, M. D.; Prenni, A. J.; Roldin, P.; Rose, D.; Schneider, J.; Su, H.; Zorn, S. R.; Artaxo, P.; Andreae, M. O. Rainforest Aerosols as Biogenic Nuclei of Clouds and Precipitation in the Amazon. *Science* **2010**, *329*, 1513−1516.
(57) Martin, S. T.; Andreae, M. O.; Althausen, D.; Artaxo, P.; Baars, H.; Borrmann, S.; Chen, Q.; Farmer, D. K.; Guenther, A.; Gunthe, S. S.; Jimenez, J. L.; Karl, T.; Longo, K.; Manzi, A.; Müller, T.; Pauliquevis, T.; Petters, M. D.; Prenni, A. J.; Pöschl, U.; Rizzo, L. V.; Schneider, J.; Smith, J. N.; Swietlicki, E.; Tota, J.; Wang, J.; Wiedensohler, A.; Zorn, S. R. An Overview of the Amazonian Aerosol Characterization Experiment 2008 (AMAZE-08). *Atmos. Chem. Phys.* **2010**, *10*, 11415−11438.
(58) Smith, N. R.; Crescenzo, G. V.; Huang, Y.; Hettiyadura, A. P. S.; Siemens, K.; Li, Y.; Faiola, C. L.; Laskin, A.; Shiraiwa, M.; Bertram, A. K.; Nizkorodov, S. A. Viscosity and Liquid−Liquid Phase Separation in Healthy and Stressed Plant SOA. *Environ. Sci.: Atmos.* **2021**, *1*, 140−153.

(59) Crittenden, J. C.; Trussel, R. R.; Hand, D. W.; Howe, K. J.; Tchobanoglous, G. *MWH's Water Treatment*; John Wiley and Sons, 2012.
(60) Faiola, C. L.; Pullinen, I.; Buchholz, A.; Khalaj, F.; Ylisirniö, A.; Kari, E.; Miettinen, P.; Holopainen, J. K.; Kivimäenpää, M.; Schobesberger, S.; Yli-Juuti, T.; Virtanen, A. Secondary Organic Aerosol Formation from Healthy and Aphid-Stressed Scots Pine Emissions. *ACS Earth Space Chem.* **2019**, *3*, 1756−1772.
(61) Lundqvist, L.; Ahlström, M. A.; Petter Axelsson, E.; Mörling, T.; Valinger, E. Multi-Layered Scots Pine Forests in Boreal Sweden Result from Mass Regeneration and Size Stratification. *For. Ecol. Manag.* **2019**, *441*, 176−181.
(62) Boratyński, A. In *Genetics of Scots Pine*; Giertych, M., Mátyás, C., Eds.; Elsevier: Budapest, 1991.
(63) Ylisirniö, A.; Buchholz, A.; Mohr, C.; Li, Z.; Barreira, L.; Lambe, A.; Faiola, C.; Kari, E.; Yli-Juuti, T.; Nizkorodov, S. A.; Worsnop, D. R.; Virtanen, A.; Schobesberger, S. Composition and Volatility of Secondary Organic Aerosol (SOA) Formed from Oxidation of Real Tree Emissions Compared to Simplified Volatile Organic Compound (VOC) Systems. *Atmos. Chem. Phys.* **2020**, *20*, 5629−5644.
(64) Ahlberg, E.; Falk, J.; Eriksson, A.; Holst, T.; Brune, W. H.; Kristensson, A.; Roldin, P.; Svenningsson, B. Secondary Organic Aerosol from VOC Mixtures in an Oxidation Flow Reactor. *Atmos. Environ.* **2017**, *161*, 210−220.
(65) McFiggans, G.; Mentel, T. F.; Wildt, J.; Pullinen, I.; Kang, S.; Kleist, E.; Schmitt, S.; Springer, M.; Tillmann, R.; Wu, C.; Zhao, D.; Hallquist, M.; Faxon, C.; Le Breton, M.; Hallquist, A. M.; Simpson, D.; Bergström, R.; Jenkin, M. E.; Ehn, M.; Thornton, J. A.; Alfarra, M. R.; Bannan, T. J.; Percival, C. J.; Priestley, M.; Topping, D.; Kiendler-Scharr, A. Secondary Organic Aerosol Reduced by Mixture of Atmospheric Vapours. *Nature* **2019**, *565*, 587−593.
(66) Faiola, C. L.; Buchholz, A.; Kari, E.; Yli-Pirilä, P.; Holopainen, J. K.; Kivimäenpää, M.; Miettinen, P.; Worsnop, D. R.; Lehtinen, K. E. J.; Guenther, A. B.; Virtanen, A. Terpene Composition Complexity Controls Secondary Organic Aerosol Yields from Scots Pine Volatile Emissions. *Sci. Rep.* **2018**, *8*, 3053−13.
(67) Angell, C. A. Relaxation in Liquids, Polymers and Plastic Crystals - Strong/Fragile Patterns and Problems. *J. Non-Cryst. Solids* **1991**, *131*−*133*, 13−31.
(68) Angell, C. A. Liquid Fragility and the Glass Transition in Water and Aqueous Solutions. *Chem. Rev.* **2002**, *102*, 2627−2650.
(69) Angell, C. A. Entropy and Fragility in Supercooling Liquids. *J. Res. Natl. Inst. Stand. Technol.* **1997**, *102*, 171−181.
(70) DeRieux, W.-S. W.; Li, Y.; Lin, P.; Laskin, J.; Laskin, A.; Bertram, A. K.; Nizkorodov, S. A.; Shiraiwa, M. Predicting the Glass Transition Temperature and Viscosity of Secondary Organic Material Using Molecular Composition. *Atmos. Chem. Phys.* **2018**, *18*, 6331−6351.
(71) Marsh, A.; Petters, S. S.; Rothfuss, N. E.; Rovelli, G.; Song, Y. C.; Reid, J. P.; Petters, M. D. Amorphous Phase State Diagrams and Viscosity of Ternary Aqueous Organic/Organic and Inorganic/Organic Mixtures. *Phys. Chem. Chem. Phys.* **2018**, *20*, 15086−15097.
(72) Rothfuss, N. E.; Petters, M. D. Characterization of the Temperature and Humidity-Dependent Phase Diagram of Amorphous Nanoscale Organic Aerosols. *Phys. Chem. Chem. Phys.* **2017**, *19*, 6532−6545.
(73) Longinotti, M. P.; Corti, H. R. Viscosity of Concentrated Sucrose and Trehalose Aqueous Solutions Including the Supercooled Regime. *J. Phys. Chem. Ref. Data* **2008**, *37*, 1503−1515.
(74) Kasparoglu, S.; Li, Y.; Shiraiwa, M.; Petters, M. Toward Closure between Predicted and Observed Particle Viscosity over a Wide Range Temperature and Relative Humidity. *Atmos. Chem. Phys.* **2021**, *21* (2), 1127−1141.
(75) de Gouw, J. A.; Brock, C. A.; Atlas, E. L.; Bates, T. S.; Fehsenfeld, F. C.; Goldan, P. D.; Holloway, J. S.; Kuster, W. C.; Lerner, B. M.; Matthew, B. M.; Middlebrook, A. M.; Onasch, T. B.; Peltier, R. E.; Quinn, P. K.; Senff, C. J.; Stohl, A.; Sullivan, A. P.; Trainer, M.; Warneke, C.; Weber, R. J.; Williams, E. J. Sources of Particulate Matter in the Northeastern United States in Summer: 1. Direct Emissions and Secondary Formation of Organic Matter in Urban Plumes. *J. Geophys. Res.* **2008**, *113*, D08301.
(76) Gao, Y.; Wang, H.; Zhang, X.; Jing, S. a.; Peng, Y.; Qiao, L.; Zhou, M.; Huang, D. D.; Wang, Q.; Li, X.; Li, L.; Feng, J.; Ma, Y.; Li, Y. Estimating Secondary Organic Aerosol Production from Toluene Photochemistry in a Megacity of China. *Environ. Sci. Technol.* **2019**, *53*, 8664−8671.
(77) Pandis, S. N.; Harley, R. A.; Cass, G. R.; Seinfeld, J. H. Secondary Organic Aerosol Formation and Transport. *Atmos. Environ., Part A* **1992**, *26*, 2269−2282.
(78) Robinson, E. S.; Saleh, R.; Donahue, N. M. Organic Aerosol Mixing Observed by Single-Particle Mass Spectrometry. *J. Phys. Chem. A* **2013**, *117*, 13935−13945.
(79) Song, M.; Maclean, A. M.; Huang, Y.; Smith, N. R.; Blair, S. L.; Laskin, J.; Laskin, A.; DeRieux, W.-S. W.; Li, Y.; Shiraiwa, M.; Nizkorodov, S. A.; Bertram, A. K. Liquid-Liquid Phase Separation and Viscosity within Secondary Organic Aerosol Generated from Diesel Fuel Vapors. *Atmos. Chem. Phys.* **2019**, *19*, 12515−12529.
(80) Gentner, D. R.; Isaacman, G.; Worton, D. R.; Chan, A. W. H.; Dallmann, T. R.; Davis, L.; Liu, S.; Day, D. A.; Russell, L. M.; Wilson, K. R.; Weber, R.; Guha, A.; Harley, R. A.; Goldstein, A. H. Elucidating Secondary Organic Aerosol from Diesel and Gasoline Vehicles through Detailed Characterization of Organic Carbon Emissions. *Proc. Natl. Acad. Sci. U.S.A.* **2012**, *109*, 18318−18323.
(81) Odum, J. R.; Jungkamp, T. P. W.; Griffin, R. J.; Flagan, R. C.; Seinfeld, J. H. The Atmospheric Aerosol-Forming Potential of Whole Gasoline Vapor. *Science* **1997**, *276*, 96−99.
(82) Velasco, E.; Lamb, B.; Westberg, H.; Allwine, E.; Sosa, G.; Arriaga-Colina, J. L.; Jobson, B. T.; Alexander, M. L.; Prazeller, P.; Knighton, W. B.; Rogers, T. M.; Grutter, M.; Herndon, S. C.; Kolb, C. E.; Zavala, M.; De Foy, B.; Volkamer, R.; Molina, L. T.; Molina, M. J. Distribution, Magnitudes, Reactivities, Ratios and Diurnal Patterns of Volatile Organic Compounds in the Valley of Mexico during the MCMA 2002 & 2003 Field Campaigns. *Atmos. Chem. Phys.* **2007**, *7*, 329−353.
(83) Velasco, E.; Pressley, S.; Grivicke, R.; Allwine, E.; Coons, T.; Foster, W.; Jobson, B. T.; Westberg, H.; Ramos, R.; Hernández, F.; Molina, L. T.; Lamb, B. Eddy Covariance Flux Measurements of Pollutant Gases in Urban Mexico City. *Atmos. Chem. Phys.* **2009**, *9*, 7325−7342.
(84) Saathoff, H.; Naumann, K.-H.; Möhler, O.; Jonsson, Å. M.; Hallquist, M.; Kiendler-Scharr, A.; Mentel, T. F.; Tillmann, R.; Schurath, U. Temperature Dependence of Yields of Secondary Organic Aerosols from the Ozonolysis of Alpha-Pinene and Limonene. *Atmos. Chem. Phys.* **2009**, *9*, 1551−1577.
(85) Li, Y. J.; Chen, Q.; Guzman, M. I.; Chan, C. K.; Martin, S. T. Second-Generation Products Contribute Substantially to the Particle-Phase Organic Material Produced by β-Caryophyllene Ozonolysis. *Atmos. Chem. Phys.* **2011**, *11*, 121−132.
(86) Hinks, M. L.; Montoya-Aguilera, J.; Ellison, L.; Lin, P.; Laskin, A.; Laskin, J.; Shiraiwa, M.; Dabdub, D.; Nizkorodov, S. A. Effect of Relative Humidity on the Composition of Secondary Organic Aerosol from the Oxidation of Toluene. *Atmos. Chem. Phys.* **2018**, *18*, 1643−1652.
(87) Malloy, Q. G. J.; Nakao, S.; Qi, L.; Austin, R.; Stothers, C.; Hagino, H.; Cocker, D. R. Real-Time Aerosol Density Determination Utilizing a Modified Scanning Mobility Particle Sizer Aerosol Particle Mass Analyzer System. *Aerosol Sci. Technol.* **2009**, *43*, 673−678.
(88) Tasoglou, A.; Pandis, S. N. Formation and Chemical Aging of Secondary Organic Aerosol during the β -Caryophyllene Oxidation. *Atmos. Chem. Phys.* **2015**, *15*, 6035−6046.
(89) Cross, E. S.; Slowik, J. G.; Davidovits, P.; Allan, J. D.; Worsnop, D. R.; Jayne, J. T.; Lewis, D. K.; Canagaratna, M.; Onasch, T. B. Laboratory and Ambient Particle Density Determinations Using Light Scattering in Conjunction with Aerosol Mass Spectrometry. *Aerosol Sci. Technol.* **2007**, *41*, 343−359.
(90) Bahreini, R.; Keywood, M. D.; Ng, N. L.; Varutbangkul, V.; Gao, S.; Flagan, R. C.; Seinfeld, J. H.; Worsnop, D. R.; Jimenez, J. L.

Measurements of Secondary Organic Aerosol from Oxidation of Cycloalkenes, Terpenes, and m-Xylene Using an Aerodyne Aerosol Mass Spectrometer. *Environ. Sci. Technol.* **2005**, *39*, 5674−5688.
(91) Ng, N. L.; Kroll, J. H.; Chan, A. W. H.; Chhabra, P. S.; Flagan, R. C.; Ng, N. L.; Kroll, J. H.; Chan, A. W. H.; Chhabra, P. S.; Flagan, R. C. Secondary Organic Aerosol Formation from M-Xylene , Toluene , and Benzene. *Atmos. Chem. Phys.* **2007**, *7*, 3909.
(92) Seinfeld, J. H.; Pandis, S. N. *Atmospheric Chemistry and Physics*, 2nd ed.; John Wiley and Sons: Hoboken, NJ, 2006.
(93) Price, H. C.; Mattsson, J.; Murray, B. J. Sucrose Diffusion in Aqueous Solution. *Phys. Chem. Chem. Phys.* **2016**, *18*, 19207−19216.
(94) Hallett, J. The Temperature Dependence of the Viscosity of Supercooled Water. *Proc. Phys. Soc.* **1963**, *82*, 1046−1050.
(95) Tsimpidi, A. P.; Karydis, V. A.; Pozzer, A.; Pandis, S. N.; Lelieveld, J. ORACLE (v1.0): Module to Simulate the Organic Aerosol Composition and Evolution in the Atmosphere. *Geosci. Model Dev.* **2014**, *7*, 3153−3172.
(96) Tsimpidi, A. P.; Karydis, V. A.; Pozzer, A.; Pandis, S. N.; Lelieveld, J. ORACLE 2-D (v2.0): An Efficient Module to Compute the Volatility and Oxygen Content of Organic Aerosol with a Global Chemistry-Climate Model. *Geosci. Model Dev.* **2018**, *11*, 3369−3389.
(97) Shiraiwa, M.; Berkemeier, T.; Schilling-Fahnestock, K. A.; Seinfeld, J. H.; Pöschl, U. Molecular Corridors and Kinetic Regimes in the Multiphase Chemical Evolution of Secondary Organic Aerosol. *Atmos. Chem. Phys.* **2014**, *14*, 8323−8341.
(98) Filippone, A. *Flight Performance of Fixed and Rotary Wing Aircraft*; Elsevier Ltd.: Oxford, 2006.
(99) Spracklen, D. V.; Jimenez, J. L.; Carslaw, K. S.; Worsnop, D. R.; Evans, M. J.; Mann, G. W.; Zhang, Q.; Canagaratna, M. R.; Allan, J.; Coe, H.; McFiggans, G.; Rap, A.; Forster, P. Aerosol Mass Spectrometer Constraint on the Global Secondary Organic Aerosol Budget. *Atmos. Chem. Phys.* **2011**, *11*, 12109−12136.
(100) Athanasiadis, A.; Fitzgerald, C.; Davidson, N. M.; Giorio, C.; Botchway, S. W.; Ward, A. D.; Kalberer, M.; Pope, F. D.; Kuimova, M. K. Dynamic Viscosity Mapping of the Oxidation of Squalene Aerosol Particles. *Phys. Chem. Chem. Phys.* **2016**, *18*, 30385−30393.
(101) Hosny, N. A.; Fitzgerald, C.; Vyšniauskas, A.; Athanasiadis, A.; Berkemeier, T.; Uygur, N.; Pöschl, U.; Shiraiwa, M.; Kalberer, M.; Pope, F. D.; Kuimova, M. K. Direct Imaging of Changes in Aerosol Particle Viscosity upon Hydration and Chemical Aging. *Chem. Sci.* **2016**, *7*, 1357−1367.
(102) Schum, S. K.; Zhang, B.; Džepina, K.; Fialho, P.; Mazzoleni, C.; Mazzoleni, L. R. Molecular and Physical Characteristics of Aerosol at a Remote Free Troposphere Site: Implications for Atmospheric Aging. *Atmos. Chem. Phys.* **2018**, *18*, 14017−14036.
(103) Champion, W. M.; Rothfuss, N. E.; Petters, M. D.; Grieshop, A. P. Volatility and Viscosity Are Correlated in Terpene Secondary Organic Aerosol Formed in a Flow Reactor. *Environ. Sci. Technol. Lett.* **2019**, *6*, 513.
(104) Saukko, E.; Lambe, A. T.; Massoli, P.; Koop, T.; Wright, J. P.; Croasdale, D. R.; Pedernera, D. A.; Onasch, T. B.; Laaksonen, A.; Davidovits, P.; Worsnop, D. R.; Virtanen, A. Humidity-Dependent Phase State of SOA Particles from Biogenic and Anthropogenic Precursors. *Atmos. Chem. Phys.* **2012**, *12*, 7517−7529.
(105) Li, Y.; Day, D. A.; Stark, H.; Jimenez, J. L.; Shiraiwa, M. Predictions of the Glass Transition Temperature and Viscosity of Organic Aerosols by Volatility Distributions. *Atmos. Chem. Phys.* **2020**, *20*, 8103−8122.
(106) Jain, S.; Fischer, K. B.; Petrucci, G. A. The Influence of Absolute Mass Loading of Secondary Organic Aerosols on Their Phase State. *Atmosphere* **2018**, *9*, 131.
(107) Tsimpidi, A. P.; Karydis, V. A.; Pandis, S. N.; Lelieveld, J. Global Combustion Sources of Organic Aerosols: Model Comparison with 84 AMS Factor-Analysis Data Sets. *Atmos. Chem. Phys.* **2016**, *16*, 8939−8962.
(108) Guenther, A.; Jiang, X.; Shah, T.; Huang, L.; Kemball-Cook, S.; Yarwood, G.; Mensink, C. Model of Emissions of Gases and Aerosol from Nature Version 3 (MEGAN3) for Estimating Biogenic Emissions. In *Air Pollution Modeling and its Application XXVI*; Gong, W., Hakami, A., Eds.; Springer International Publishing: Cham, 2020; pp 187−192.
(109) Song, M.; Liu, P. F.; Hanna, S. J.; Li, Y. J.; Martin, S. T.; Bertram, A. K. Relative Humidity-Dependent Viscosities of Isoprene-Derived Secondary Organic Material and Atmospheric Implications for Isoprene-Dominant Forests. *Atmos. Chem. Phys.* **2015**, *15*, 5145−5159.
(110) Ditto, J. C.; Joo, T.; Khare, P.; Sheu, R.; Takeuchi, M.; Chen, Y.; Xu, W.; Bui, A. A. T.; Sun, Y.; Ng, N. L.; Gentner, D. R. Effects of Molecular-Level Compositional Variability in Organic Aerosol on Phase State and Thermodynamic Mixing Behavior. *Environ. Sci. Technol.* **2019**, *55*, 13009.
(111) Bateman, A. P.; Gong, Z.; Liu, P.; Sato, B.; Cirino, G.; Zhang, Y.; Artaxo, P.; Bertram, A. K.; Manzi, A. O.; Rizzo, L. V.; Souza, R. A. F.; Zaveri, R. A.; Martin, S. T. Sub-Micrometre Particulate Matter Is Primarily in Liquid Form over Amazon Rainforest. *Nat. Geosci.* **2016**, *9*, 34−37.
(112) Ye, Q.; Robinson, E. S.; Ding, X.; Ye, P.; Sullivan, R. C.; Donahue, N. M. Mixing of Secondary Organic Aerosols versus Relative Humidity. *Proc. Natl. Acad. Sci. U.S.A.* **2016**, *113*, 12649−12654.
(113) Pajunoja, A.; Hu, W.; Leong, Y. J.; Taylor, N. F.; Miettinen, P.; Palm, B. B.; Mikkonen, S.; Collins, D. R.; Jimenez, J. L.; Virtanen, A. Phase State of Ambient Aerosol Linked with Water Uptake and Chemical Aging in the Southeastern US. *Atmos. Chem. Phys.* **2016**, *16*, 11163−11176.
(114) Bateman, A. P.; Gong, Z.; Harder, T. H.; de Sá, S. S.; Castillo, P.; China, S.; Liu, Y.; O'Brien, R. E.; Palm, B. B.; Shiu, H.-W.; Cirino, G. G.; Thalman, R.; Adachi, K.; Alexander, M. L.; Artaxo, P.; Bertram, A. K.; Buseck, P. R.; Gilles, M. K.; Jimenez, J. L.; Laskin, A.; Manzi, A. O.; Sedlacek, A.; Souza, R. A. F.; Wang, J.; Zaveri, R.; Martin, S. T.; Martin, S. T. Anthropogenic Influences on the Physical State of Submicron Particulate Matter over a Tropical Forest. *Atmos. Chem. Phys.* **2017**, *17*, 1759−1773.
(115) Carlson, T. N. Speculations on the Movement of Polluted Air to the Arctic. *Atmos. Environ.* **1981**, *15*, 1473−1477.
(116) Weinzierl, B.; Ansmann, A.; Prospero, J. M.; Althausen, D.; Benker, N.; Chouza, F.; Dollner, M.; Farrell, D.; Fomba, W. K.; Freudenthaler, V.; Gasteiger, J.; Groß, S.; Haarig, M.; Heinold, B.; Kandler, K.; Kristensen, T. B.; Mayol-Bracero, O. L.; Müller, T.; Reitebuch, O.; Sauer, D.; Schäfler, A.; Schepanski, K.; Spanu, A.; Tegen, I.; Toledano, C.; Walser, A. The Saharan Aerosol Long-Range Transport and Aerosol-Cloud-Interaction Experiment: Overview and Selected Highlights. *Bull. Am. Meteorol. Soc.* **2017**, *98*, 1427−1451.
(117) Zhao, Z.; Cao, J.; Shen, Z.; Xu, B.; Zhu, C.; Chen, L. W. A.; Su, X.; Liu, S.; Han, Y.; Wang, G.; Ho, K. Aerosol Particles at a High-Altitude Site on the Southeast Tibetan Plateau, China: Implications for Pollution Transport from South Asia. *J. Geophys. Res. Atmos.* **2013**, *118*, 11360−11375.
(118) Zelenyuk, A.; Imre, D.; Beránek, J.; Abramson, E.; Wilson, J.; Shrivastava, M. Synergy between Secondary Organic Aerosols and Long-Range Transport of Polycyclic Aromatic Hydrocarbons. *Environ. Sci. Technol.* **2012**, *46*, 12459−12466.
(119) Mu, Q.; Shiraiwa, M.; Octaviani, M.; Ma, N.; Ding, A.; Su, H.; Lammel, G.; Pöschl, U.; Cheng, Y. Temperature Effect on Phase State and Reactivity Controls Atmospheric Multiphase Chemistry and Transport of PAHs. *Sci. Adv.* **2018**, *4*, No. eaap7314.
(120) Shrivastava, M.; Lou, S.; Zelenyuk, A.; Easter, R. C.; Corley, R. A.; Thrall, B. D.; Rasch, P. J.; Fast, J. D.; Massey Simonich, S. L.; Shen, H.; Tao, S. Global Long-Range Transport and Lung Cancer Risk from Polycyclic Aromatic Hydrocarbons Shielded by Coatings of Organic Aerosol. *Proc. Natl. Acad. Sci. U.S.A.* **2017**, *114*, 1246−1251.
(121) Friedman, C. L.; Pierce, J. R.; Selin, N. E. Assessing the Influence of Secondary Organic versus Primary Carbonaceous Aerosols on Long-Range Atmospheric Polycyclic Aromatic Hydrocarbon Transport. *Environ. Sci. Technol.* **2014**, *48*, 3293−3302.
(122) Heald, C. L.; Jacob, D. J.; Turquety, S.; Hudman, R. C.; Weber, R. J.; Sullivan, A. P.; Peltier, R. E.; Atlas, E. L.; de Gouw, J. A.; Warneke, C.; Holloway, J. S.; Neuman, J. A.; Flocke, F. M.; Seinfeld, J.

H. Concentrations and Sources of Organic Carbon Aerosols in the Free Troposphere over North America. *J. Geophys. Res. Atmos.* **2006**, *111*, D23S47.
(123) Holopainen, J. K.; Virjamo, V.; Ghimire, R. P.; Blande, J. D.; Julkunen-Tiitto, R.; Kivimäenpää, M. Climate Change Effects on Secondary Compounds of Forest Trees in the Northern Hemisphere. *Front. Recent Dev. Plant Sci.* **2018**, *9*, 1445.
(124) Li, T.; Holst, T.; Michelsen, A.; Rinnan, R. Amplification of Plant Volatile Defence against Insect Herbivory in a Warming Arctic Tundra. *Nat. Plants* **2019**, *5*, 568−574.
(125) Werner, C.; Fasbender, L.; Romek, K. M.; Yáñez-Serrano, A. M.; Kreuzwieser, J. Heat Waves Change Plant Carbon Allocation Among Primary and Secondary Metabolism Altering CO2 Assimilation, Respiration, and VOC Emissions. *Front. Recent Dev. Plant Sci.* **2020**, *11*, 1242.
(126) Centeno, G.; Sánchez-Reyna, G.; Ancheyta, J.; Muñoz, J. A. D.; Cardona, N. Testing Various Mixing Rules for Calculation of Viscosity of Petroleum Blends. *Fuel* **2011**, *90*, 3561−3570.
(127) Rovelli, G.; Song, Y.-C.; MacLean, A. M.; Topping, D. O.; Bertram, A. K.; Reid, J. P. Comparison of Approaches for Measuring and Predicting the Viscosity of Ternary Component Aerosol Particles. *Anal. Chem.* **2019**, *91*, 5074−5082.
(128) Song, Y. C.; Haddrell, A. E.; Bzdek, B. R.; Reid, J. P.; Bannan, T.; Topping, D. O.; Percival, C.; Cai, C. Measurements and Predictions of Binary Component Aerosol Particle Viscosity. *J. Phys. Chem. A* **2016**, *120*, 8123−8137.
(129) Zhang, Y.; Chen, Y.; Lei, Z.; Olson, N. E.; Riva, M.; Koss, A. R.; Zhang, Z.; Gold, A.; Jayne, J. T.; Worsnop, D. R.; Onasch, T. B.; Kroll, J. H.; Turpin, B. J.; Ault, A. P.; Surratt, J. D. Joint Impacts of Acidity and Viscosity on the Formation of Secondary Organic Aerosol from Isoprene Epoxydiols (IEPOX) in Phase Separated Particles. *ACS Earth Space Chem.* **2019**, *3*, 2646−2658.
(130) Riva, M.; Chen, Y.; Zhang, Y.; Lei, Z.; Olson, N. E.; Boyer, H. C.; Narayan, S.; Yee, L. D.; Green, H. S.; Cui, T.; Zhang, Z.; Baumann, K.; Fort, M.; Edgerton, E.; Budisulistiorini, S. H.; Rose, C. A.; Ribeiro, I. O.; e Oliveira, R. L.; Dos Santos, E. O.; Machado, C. M. D.; Szopa, S.; Zhao, Y.; Alves, E. G.; de Sá, S. S.; Hu, W.; Knipping, E. M.; Shaw, S. L.; Duvoisin Junior, S.; De Souza, R. A. F.; Palm, B. B.; Jimenez, J.-L.; Glasius, M.; Goldstein, A. H.; Pye, H. O. T.; Gold, A.; Turpin, B. J.; Vizuete, W.; Martin, S. T.; Thornton, J. A.; Dutcher, C. S.; Ault, A. P.; Surratt, J. D. Increasing Isoprene Epoxydiol-to-Inorganic Sulfate Aerosol Ratio Results in Extensive Conversion of Inorganic Sulfate to Organosulfur Forms: Implications for Aerosol Physicochemical Properties. *Environ. Sci. Technol.* **2019**, *53*, 8682−8694.
(131) Hornbuckle, B. K.; England, A. W. Diurnal Variation of Vertical Temperature Gradients within a Field of Maize: Implications for Satellite Microwave Radiometry. *IEEE Geosci. Remote. Sens. Lett.* **2005**, *2*, 74−77.
(132) Liu, P. F.; Zhao, C. S.; Göbel, T.; Hallbauer, E.; Nowak, A.; Ran, L.; Xu, W. Y.; Deng, Z. Z.; Ma, N.; Mildenberger, K.; Henning, S.; Stratmann, F.; Wiedensohler, A. Hygroscopic Properties of Aerosol Particles at High Relative Humidity and Their Diurnal Variations in the North China Plain. *Atmos. Chem. Phys.* **2011**, *11*, 3479−3494.
(133) Chepfer, H.; Brogniez, H.; Noel, V. Diurnal Variations of Cloud and Relative Humidity Profiles across the Tropics. *Sci. Rep.* **2019**, *9*, 16045−9.
(134) Chung, E. S.; Sohn, B. J.; Schmetz, J.; Koenig, M. Diurnal Variation of Upper Tropospheric Humidity and Its Relations to Convectiye Activities over Tropical Africa. *Atmos. Chem. Phys.* **2007**, *7*, 2489−2502.
(135) Foltz, G. S.; Gray, W. M. Diurnal Variation in the Troposphere's Energy Balance. *J. Atmos. Sci.* **1979**, *36*, 1450−1466.

https://doi.org/10.1021/acsearthspacechem.1c00296
ACS Earth Space Chem. 2021, 5, 3458−3473